

1 Late Cretaceous to Early Cenozoic Initiation of Rifting of the  
2 Windhoek Graben, Namibia

3

4 **R. Waren**

5 Department of Earth Sciences, University of Oxford, South Parks Road, Oxford, OX1 3AN, UK

6 email: reybi.waren@sjc.ox.ac.uk

7 **J. A. Cartwright**

8 Department of Earth Sciences, University of Oxford, South Parks Road, Oxford, OX1 3AN, UK

9 email: joe.cartwright@earth.ox.ac.uk

10 **M. C. Daly**

11 Department of Earth Sciences, University of Oxford, South Parks Road, Oxford, OX1 3AN, UK

12 email: mike.daly@earth.ox.ac.uk

13 **R. Swart**

14 BlackGold Geosciences, Windhoek 24287, Namibia

15 email: rogerswart@afol.com.na

16

17 **ABSTRACT**

18         The Windhoek Graben is a N-S trending rift in central Namibia that forms a prominent  
19 topographic feature bisecting an area of plateau uplift. It occupies a potentially crucial role in the  
20 propagation of the Late Cenozoic Southwest African Rift system regarding a possible continuation  
21 to the west of the Eiseb Rift. It is an unusual example of intra-continental rifting because it has no  
22 significant sediment fill associated with the period of active rifting, and hence the timing of rift

23 activity nor its tectonic relevance has not hitherto been established. To constrain the age of the  
24 Windhoek Graben we examine its regional geomorphic context and its relationship to four sites of  
25 igneous activity in the central Namibian Highlands. Two of these consist of clusters of eroded  
26 phonolitic tholoid bodies that have yielded  $^{40}\text{Ar}/^{39}\text{Ar}$  dates of 32 Ma and 52 Ma, respectively, that  
27 we use to bracket the age of formation of a prominent remnant land surface, termed here the P52  
28 Surface. From previous mapping of older intrusive igneous bodies, we argue that an even older  
29 land surface is partially preserved on the highest features in the area, and this surface (termed PRS)  
30 defines an initial domally uplifted surface from which initial drainage radiated, and onto which the  
31 earliest volcanic products associated with the Graben were erupted. In particular, the strong  
32 similarity in dyke and fault orientations is used to argue for a causal connection between the earliest  
33 magmatic activity and the onset of rifting. Long range correlation of PRS into the adjacent Aranos  
34 Basin strongly suggests a Late Cretaceous age for this earliest magmatic activity and the onset of  
35 rifting, but we cannot exclude a younger origin, any time up to the Early Eocene.

36

## 37 1. INTRODUCTION

38 Our study focus is the Windhoek Graben in central Namibia (Fig.1). This relatively  
39 immature rift basin is unusual in a global context, in that it is almost devoid of a graben fill (Miller,  
40 2008; Picart et al., 2020). As a result, there is no syn-rift stratigraphy preserved with which to  
41 frame a chronostratigraphic evolution (Rosendahl et al., 1986; Morley, 1988; Leeder and Jackson,  
42 1993). Hence there are open questions as to the timing of graben formation, which is important to  
43 resolve the geodynamic context for rifting in this part of southern Africa (Daly et al., 2020).

44 The main aim of this paper is to attempt to place age constraints on the initiation of rifting  
45 of the Windhoek Graben where the lack of a preserved syn-rift succession prevents a more

46 conventional analysis used for dating rift onset in many other rift basins. Instead, we focus on  
47 using geomorphological arguments and, more specifically, attempt to reconstruct the development  
48 of former land surfaces as proxies for chronostratigraphic datums. Our approach is based on our  
49 own primary interpretation of the present day relief of the Windhoek Graben and surrounding  
50 Namibian Highlands combined with a synthesis of previous geological and geomorphological  
51 mapping undertaken over many decades. Particularly significant, is the inclusion of a review of  
52 the post-Jurassic igneous activity in the study area, which proved to be instrumental in providing  
53 age constraints for the older, partially preserved land surfaces.

54 We emphasise that our focus here is specifically on the critical and unresolved question of  
55 rift initiation, rather than on subsequent rift evolution. Future work will address the rift kinematics  
56 in a broader geodynamic context. Although beyond the scope of this paper, the ultimate question  
57 of the geodynamic context for rifting can only be addressed once the timing of rifting is better  
58 constrained. This may, for example, ultimately allow recent suggestions by Daly et al. (2020) of  
59 the propagation of a through-going rift system from the East African Rift, across central Africa to  
60 Namibia to be tested, at least in the area of central Namibia.

61

## 62 **2. PREVIOUS INTERPRETATIONS OF THE WINDHOEK GRABEN**

63 The origin and evolution of the Windhoek Graben have received relatively little attention  
64 considering its potential significance in the wider tectonic evolution of Namibia. It was first  
65 discussed as a possible graben nearly 100 years ago. Gevers (1942) notes that the linear  
66 morphology of the ‘Windhoek Valley’ is reminiscent of the graben structure interpreted by ‘early  
67 pioneering geologists’ but then went on to argue that the lack of obvious displacement of  
68 stratigraphic markers in the basement rocks bordering the valley argued against this interpretation.

69 Gevers (1942) referred to N-S trending silicified breccia zones as being connected to the volcanic  
70 plugs of the Auas Mountains, and his early mapping (Gevers, 1932) of these zones included a  
71 number of small faults that strike between NW and SE in the area just south of Windhoek. It was  
72 almost 30 years later that these faults were mapped in more detail as part of a wider mapping  
73 program aimed at unravelling the structure of the Damaran complexes (Guj, 1967).

74 The Windhoek Graben and its near neighbour, the Swakop Graben (Fig.2), have been  
75 identified and mapped as part of the regional geological mapping of Namibia (Namibia Geological  
76 Map 1:1,000,000). This map shows prominent normal faults oriented broadly N-S extending some  
77 100 km from south of Windhoek and bordering both sides of the prominent linear topographic  
78 depression described by Gevers (1942) (Fig.2B). The southern part of the Windhoek Graben was  
79 mapped in greater detail by Miller and Schalk (1980) and at 1:50,000 by Hoffmann and Schreiber  
80 (2011) who identified sets of NNW and NNE trending extensional faults across a 12 km wide  
81 transect (Fig. 3). These faults were identified from a combination of groundwater exploration  
82 borehole data and surface mapping, in which highly fractured and cemented fault zone breccias  
83 provided direct indications of the presence of a fault. Miller (2008) reviewed the previous mapping  
84 efforts in the area, and presented summary maps showing normal faults bordering the Windhoek  
85 Graben extending continuously for 120 km to the north of Okahandja (town). Most recently,  
86 groundwater investigations using deep-penetrating electrical resistivity surveys have added further  
87 details on the fault distribution in the area of Windhoek, including detailed petrological studies of  
88 the silicified fault breccias and a discussion of fault dips (Miller et al., 2018).

89 An important contribution with implications for the origin of the Windhoek Graben was a  
90 subsurface and surface mapping study made by Hartmann (1994), of the area surrounding the  
91 Otjihase Mine. This mine is located in the mountainous region 20 km NE of Windhoek (Fig. 3),

92 where a prominent ore body associated with base metal sulfide mineralization of the Matchless  
93 Amphibolite is offset systematically downwards by a series of N-S striking, steeply west-dipping  
94 normal faults with displacements ranging from 50-230 m. The Hoffnung Fault is the largest of  
95 these with a recorded value of 230 m total displacement with a dip of c.60 degrees to the west and  
96 is associated with a prominent eroded fault plane scarp at the surface. These faults are step or  
97 terrace faults located within the footwall to and synthetic with the eastern bounding fault (Fig. 3).  
98 Offsets of the Matchless Amphibolite across the main graben bounding fault (Fig. 3B) suggests a  
99 total displacement of c. 1000 m (Miller, R, pers comm).

100 Previous discussion of the age of the Windhoek Graben has been limited to two brief  
101 references. Mvondo et al. (2011) briefly state that the graben was ‘associated to phonolite  
102 intrusions of Paleocene’. Most recently, Picart et al. (2020) mapped planation surfaces over a large  
103 area of central Namibia. From their mapping of a surface referred to as S6, which they interpreted  
104 as forming the floor of the Windhoek Graben, they suggest that the graben was formed prior to the  
105 development of this key surface in the middle Eocene.

106

### 107 **3. REGIONAL CONTEXT**

#### 108 **3.1. Physiographical Setting**

109 The Windhoek Graben lies in an arid climatic zone, where annual rainfall is < 350 mm,  
110 and this arid to semi-arid climate regime can be inferred for the area back into the Mid Cenozoic  
111 (Ward, 1988). The relative aridity also means that there is good preservation of the vestiges of  
112 former land surfaces on the elevated margins surrounding the topographic depression representing  
113 the graben floor (Gevers, 1942; Mabbutt, 1951; Martin, 1973). These have the potential to be used

114 as datums for dating the formation of the Windhoek Graben, provided there are objective criteria  
115 to date them or at least to identify them as specific to a particular erosional episode.

116         The Windhoek and Swakop Grabens are located in a region known as the Namibian  
117 Highlands (Fig.2). This elevated plateau reaches altitudes above 2000 m with some notable ridges  
118 rising to nearly 2500 m just south-east of Windhoek and some 500 m above the regional land  
119 surface. The surface is deeply dissected by a diversity of drainage networks, from large valleys  
120 linked to the major rivers, to smaller, trellis-like drainage networks dissecting the flank regions of  
121 the graben, forming a deeply dissected plateau. The Namibian Highlands are bordered to the east  
122 by the extensive interior plateau region (Haddon and McCarthy, 2005), which, in the southeast, is  
123 floored by the Aranos Basin and is marked by a much smoother topography, excluding the few  
124 valleys cut by the major rivers, and with a regional elevation of between 1150 and 1200 m. To the  
125 west of the Namibian Highlands, the highly dissected land surface slopes down to the Great  
126 Escarpment (trending N-S at approximately 16°E, Fig. 2A).

127         To the north of the Swakop River, the Great Escarpment ceases to have any noticeable  
128 physiographic expression, possibly as a consequence of the collective erosional action of the major  
129 rivers that rise at the continental watershed and flow into the Atlantic Ocean, namely, the Swakop,  
130 Omaruru, and Ugab rivers (Aizawa et al., 2000). A prominent dissected scarp running  
131 approximately along the trace of the Okahandja Lineament demarcates the northern limit of the  
132 Namibian Highlands. This scarp has been partly cut by the Swakop River and forms the southern  
133 valley margin of that river, but it also represents a flexure or hinge line plunging northwards,  
134 possibly exploiting the basement weaknesses. Gevers (1942) and Mabbutt (1951) both recognized  
135 this flexure and Gevers (1942) considered it to be Mid Cretaceous in age.

136           The southern margin of the Namibian Highlands is marked by a prominent series of ridges  
137 striking parallel to the Damaran structural grain dissected to varying degrees by south or south-  
138 east flowing rivers. These ridges have been described as relict form to a former landsurface with  
139 the characteristics of accordant summits that comprise the more resistant rock types (Gevers,  
140 1942). The valley floors of rivers such as the Usib and Nossob cut through these ridges and descend  
141 over a distance of 200 km to the lower relief of the interior plateau to the south and east (Fig.2A).  
142 A number of partially or almost completely preserved phonolitic extrusive bodies and associated  
143 vents form two important igneous clusters referred to here as the Aris and Stalhart Clusters,  
144 described in detail in Marsh (2010). These have been dated, and since these volcanic edifices were  
145 erupted onto a land surface that is interpreted to be close to the present day valley floors of rivers  
146 rising in the Namibian Highlands, they form a principal means for dating the erosion by those  
147 rivers.

148           The major drainages in the region of central Namibia are arranged in a strikingly radial  
149 pattern centered on the Namibian Highlands (Fig. 2A). Six major catchment areas can be defined  
150 with irregular, spoke-like drainage divides separating them. West flowing rivers such as the  
151 Swakop and Kuiseb cross the Great Escarpment and flow into the Atlantic (Matmon et al., 2018).  
152 South and southeast flowing rivers such as the Usib and Nossob flow into the Kalahari Basin or as  
153 tributaries to join the Fish River. North flowing rivers (e.g., Omatako River) flow into the  
154 Okavango River and represent examples of interior plateau drainage. This radial pattern of  
155 drainage is clearly consequent upon the topographic elevation of the Namibian Highlands, and  
156 hence understanding the erosional history of these rivers is a critical step in reconstructing the  
157 uplift history of the region.

158           One of the subtler features of this radial drainage system is the pattern of tributary drainage  
159 into the Swakop River (Fig. 2B). The Swakop River is remarkably linear over much of its course,  
160 rising near the main continental drainage divide northeast of Okahandja, and maintaining a WSW-  
161 oriented course over its 360 km journey to the sea. Near its headwaters, two tributaries join the  
162 main trunk river almost orthogonally from the south, and these tributaries form prominent axial  
163 drainages along the Windhoek and Swakop Grabens. This geometrical relationship between major  
164 faulted structures and the tributaries strongly suggests consequent drainage evolution, but without  
165 any obvious signs of river capture. This further suggests that the timing of formation of tributary  
166 drainages postdates that of the structural control.

### 167 **3.2. Geological Setting**

168           The Windhoek Graben is located within the Damaran orogenic belt (Miller, 1983). The  
169 basement geology encompassing the Windhoek Graben is dominated by schists of the Swakop  
170 Group of the Neoproterozoic Damara Supergroup (e.g., Miller, 2008). These originated as shelf-  
171 slope successions deposited on the continental margin bordering a small ocean basin (Martin and  
172 Porada, 1977; Downing and Coward, 1981). These sediments were metamorphosed and deformed  
173 by closure of this ocean basin during the Late Proterozoic to Cambrian (Barnes and Sawyer, 1980;  
174 de Kock, 1992). The dominant SE vergence of this collisional orogenesis led to the formation of  
175 crustal-scale shear zones and thrusts (Fig. 4A and B) that locally emplaced fragments of the old  
176 oceanic crust (the Matchless Amphibolite) at a shallow level on the highly deformed continental  
177 margin succession (Hoffmann, 1983; Miller, 1983; Kukla, 1992). Towards the southern end of the  
178 Windhoek Graben, the original coarser facies of the continental margin succession is preserved as  
179 a series of thick quartzite units (Guj, 1967) and these form prominent ridges in the modern  
180 landscape due to their erosional resistance (Gevers, 1942) (Fig. 4C).



181           The shear zones and thrusts exposed at surface in central Namibia have a predominant NE-  
182 SW strike. Of these, the most prominent is the Okahandja Lineament (OKL) which extends for  
183 about 650 km along the southern limit of the central tectonostratigraphic zone (Miller, 1983) (Fig.  
184 4A). Surface deformational evidence of late-stage, multiphase strike-slip kinematics has been  
185 documented along portions of the OKL (Downing and Coward, 1981), that is interpreted as a  
186 former prism backstop, with a near-vertical geometry extending across the full thickness of the  
187 present-day crust (Kukla, 1992) (Fig. 4B).

188           Further to the southeast is the more curvilinear, but broadly SW-NE trending Us Pass  
189 Lineament (UPL), which defines the southernmost limit of the Southern Tectonostratigraphic Zone  
190 of the orogen (Miller, 1983) (Fig. 4A). This complex zone of thrusting comprises a number of  
191 thrusts, and imbricate splays exposing Paleo- to Mesoproterozoic basement (Miller and Schalk,  
192 1980; Miller, 1983). The UPL has been interpreted as a continental suture zone (Hoffmann, 1983),  
193 forming a thrust zone dipping to the NW in the subsurface (Kukla, 1992) (Fig. 4B). Intense activity  
194 of the late-stage collisional tectonics also contributed to the emplacement of large bodies of granite  
195 during the Late Precambrian to Cambrian (Barnes and Sawyer, 1980; Downing and Coward, 1981;  
196 Porada, 1989; de Kock, 1992; Gray et al., 2008).

197           Preservation of younger successions is limited to outliers of the Karoo Supergroup (Late  
198 Carboniferous to Early Jurassic) in the north and south of the area, and to a more substantial  
199 outcrop of the Nama Supergroup (Cambrian) in the southwestern limit of the study area (Fig. 4A).  
200 This outcrop represents the northern margin of a large foreland basin in which the Nama Group  
201 accumulated.

202           The later geological and geomorphological evolution of this region has been substantially  
203 influenced by the break-up of Gondwana to form the South Atlantic Ocean during the Early

204 Cretaceous, resulting in the formation of the Namibian Volcanic Margin (Clemson et al., 1997;  
205 Gladchenko et al., 1997). This rifting process was followed by a significant uplift and erosional  
206 event along the margin in the Late Cretaceous to Middle Eocene (Partridge and Maud, 1987;  
207 Partridge, 1998; Gallagher and Brown, 1999; Aizawa et al., 2000; Bluck et al., 2007; Burke and  
208 Gunnell, 2008). A major erosional event in the Late Cretaceous has also been inferred by Miller  
209 (2008) based on a reconstruction of the stratigraphic evolution of the Aranos Basin derived from  
210 correlation of hundreds of groundwater boreholes. The Aranos Basin is a well-defined depocenter  
211 within the broader Kalahari Basin (Fig. 4A). Miller (2008) correlated lateritized intervals of  
212 remnant Karoo to demonstrate that these Karoo sediments were highly dissected to 200-300 m  
213 below the present-day surface by an extensive river system (referred to by Miller (2008) as the  
214 Aranos River) flowing S-SE to the palaeo-Orange River, via the palaeo-Molopo River during the  
215 Late Cretaceous. The Late Cretaceous initiation of this river system, therefore, implies that a south-  
216 eastward surface topographic gradient was established in this area at this time.

217         The Cenozoic history of the study area is poorly understood. The area has been shaped by  
218 a number of processes including: regional-scale uplift events (Picart et al., 2020), infill of the  
219 Aranos Basin and calcrete development beneath a younger aeolian cover (Miller, 2008), igneous  
220 activity (Ferreira et al., 1979; Marsh, 2010), and fluvial incision (Gevers, 1942; Mabbutt, 1951).  
221 Uplift events cited in previous studies vary in their timing, magnitude, and origin. For example, a  
222 Late Cretaceous/Paleocene uplift event was attributed to lingering plume tails after Gondwana  
223 breakup (Nyblade and Sleep, 2003) and is supported by palaeo-topographic reconstructions of  
224 Aizawa et al. (2000), Bluck et al. (2007), and by apatite fission-track studies (Raab et al., 2002).  
225 In contrast, regional uplift of southern Africa in the Oligocene–Miocene was linked to an African  
226 superplume (Burke, 1996) or lithospheric bulge (e.g., Picart et al., 2020). A more local uplift

227 occurred in the Bie Dome (located some 500 km north of the study area) during the Pliocene–  
228 Pleistocene, and has been linked to a secondary plume (e.g., Al-Hajri et al., 2009).

229 In considering any possible mantle involvement in the uplift history of the region, it is  
230 worth noting the occurrence of a number of igneous complexes in the study area. These include  
231 the Stalhart cluster of phonolites, the Aris cluster of phonolites/trachytes, and the Regenstein vent  
232 complex and associated trachyte plugs and breccia dykes (Gevers, 1932; Burger and Walraven,  
233 1976; Ferreira et al., 1979; Marsh, 2010). The first two are dated (52 and 32 Ma, respectively), but  
234 the ages of the Regenstein vent complex and associated trachyte dykes are unconstrained due to  
235 severe alteration (Ferreira et al., 1979). The Stalhart and Aris igneous bodies provide some  
236 constraints on the rate and style of erosional processes (Marsh, 2010) but also testify to a  
237 potentially significant early to mid-Cenozoic phase of magmatism. A suite of largely phonolitic  
238 extrusive bodies dated at 46 Ma is well described from the Klinghardt Mountains (Marsh et al.,  
239 2018), on the coastal plain 520 km to the southwest of the study area. The occurrence of younger  
240 sediments is restricted to the Aranos Basin and to the coastal plain where Late Cenozoic to Recent  
241 aeolian sediments several hundred meters thick have accumulated over the highly eroded basement  
242 rocks of the coastal Damaran and Gariiep orogenic belts (Ward, 1988; Haddon and McCarthy,  
243 2005).

244

#### 245 **4. DATA AND METHODOLOGY**

246 The paper initially focuses on reviewing published works related to the occurrence of four  
247 suites of igneous rocks and their relationship to both the graben structure and the geomorphology  
248 in order to establish key landsurfaces. We correlate key surfaces from the Windhoek area down to  
249 the neighbouring Aranos basin to the south (Fig.2), where hundreds of groundwater boreholes have

250 proved helpful in reconstructing the age of fluvial dissection (Miller, 2008). This approach  
251 generates a chronological framework, which is used to constrain the initiation age of rifting.

252 We describe the regional topography and geomorphology in the immediate area  
253 surrounding the Windhoek Graben using a DEM of the study area (SRTM 30) to compute  
254 topographic profiles, identify drainage basins and characterise the surface morphology.  
255 Topographic profiles were interpreted based on previous studies that discuss the landforms  
256 occurring along specific transects. Correlations of possible palaeo-surfaces are explained in the  
257 results section. Faults were identified and extracted from published geological maps of 1:250,000  
258 (sheet 2116 and 2216, Geological Survey of Namibia) and 1: 1,000,000 (Miller and Schalk, 1980),  
259 and 1:50,000 (Hoffmann and Schreiber, 2011), and other published sources available (Guj, 1967;  
260 Ferreira et al., 1979; Hartmann, 1994; Miller, 2008; Miller et al., 2018; Picart et al., 2020) and  
261 incorporated into a GIS framework (ArcMap 10.8© and Global Mapper v21.0©). Additional faults  
262 were interpreted based on recognizing fault scarps using standard criteria developed for rift  
263 tectonic geomorphological analysis (e.g., Gawthorpe and Leeder, 2000; Goldsworthy and Jackson,  
264 2000). The interpretation was validated by cross-referencing the DEM with the published  
265 geological maps to identify and eliminate any linear scarps that could be attributed to lithological  
266 boundaries.

267 We compiled maps showing the distribution of the igneous suites utilizing a published map  
268 by Miller (2008) that is compiled from Gevers (1934), Guj (1967), Ferreira et al. (1979), Hoffmann  
269 (1983), Niku-Paalova (1997), and Hoffman and Schreiber (1998). We carried out fieldwork to  
270 verify the descriptions of all igneous suites by Gevers (1934), Ferreira et al. (1979), and Marsh  
271 (2010) to understand their genetic, spatial, and temporal relationships to the present-day surface,  
272 and additionally, to the graben.

273 We reconstructed the positions of two key palaeo-surfaces in the southern Windhoek area  
274 by constructing profiles across and between the dated igneous bodies. Identification of the oldest  
275 former land surface was based heavily on the previous interpretation of river superposition to form  
276 narrow gorges through the resistant ridges that occur south of Windhoek (details in following  
277 sections). Further constraints on the age of the oldest surface were derived from projections of the  
278 key reconstructed surfaces into the subsurface of the Aranos Basin along a ~400 km topographic  
279 profile (SRTM 30), taking into account the basin configuration of Miller (2008).

280 Recent mapping of planation surfaces has been undertaken by Picart et al. (2020) over  
281 southern Namibia, extending as far north as the Windhoek Graben. They interpreted the remnants  
282 of eight discrete surfaces, which in their interpretation are suggested to have formed at different  
283 times, sequentially from S0 (oldest) to S8 (youngest). In our study area, the oldest surfaces  
284 identified by Picart et al. (2020) (S0, S1 and S2) are not dated. S3 is argued to post-date the  
285 ‘Rehoboth phonolites’ and hence is of Middle Eocene age. The floor of the Windhoek Graben is  
286 mapped as surface S6, which Picart et al. (2020) dated as Early Miocene by long range correlation  
287 to the outcrops of the Middle Miocene in the Namib Desert. Relationships between these surfaces  
288 and our reconstructed surfaces are considered further in the Discussion.

## 289 **5. RESULTS**

### 290 **5.1. Tectonic Geomorphology of The Windhoek Graben**

291 Prominent escarpments are developed along the western and eastern margins of the  
292 Windhoek Graben, particularly in the central and northern areas (Fig.4). The mapped position of  
293 the major bounding faults of the graben coincides with the bases of both the eastern and western  
294 escarpments and, on this basis, both escarpments can be interpreted as eroded fault scarps (cf.,  
295 Wallace, 1977) (Fig.5A).

296 In detail, the morphology of the two bounding fault scarps differs considerably. The eastern  
297 scarp conforms more classically to a highly degraded normal fault scarp, with a generalized dip of  
298 between 1.7 and 2.0 degrees up to a prominent ridge separating the scarp from the relatively  
299 undissected, gently east-dipping footwall dip slope (Fig. 3A). The topographic elevation difference  
300 of the crest of the scarp with respect to the graben floor elevation varies systematically along strike  
301 reaching a maximum value approximately midway along the length of the fault, with an elevation  
302 difference of c. 600 m. Scarp drainages are spaced every kilometer or so along strike, and exploit  
303 local heterogeneities in the basement rocks of the footwall. These short-headed rivers flow with  
304 stepped profiles down to the base of the scarp at the hanging wall cutoff (Fig. 5B). The strike of  
305 the scarp is generally NNE-SSW in the central area, but changes across a series of segment  
306 boundaries or relay structures toward the northern area, where it trends NNW-SSE. These changes  
307 of strike, and in some cases of lateral offset of the base of the scarp, allow the entire structure to  
308 be sub-divided into a number of segments, bounded by relay structures. These relay structures  
309 appear to have been breached at an early stage in the displacement history of the bounding fault  
310 and are now fully hard-linked (cf., Trudgill and Cartwright, 1994). The breached relays are loci  
311 for the more prominent scarp drainages, often with the largest catchment areas of any of the scarp  
312 drainages. The scarp drainages feed as tributaries into the main axial drainage of the graben floor,  
313 and locally grade into the profile of this axial river (Fig. 5C). However, the axial river does not  
314 incise or behead any of these tributary streams, and there is no evidence that the axial river has cut  
315 significantly downwards into the relatively smooth topography of the graben floor. Fresh triangular  
316 facets, waterfalls, or beheaded spurs are not found along the footwall scarps, suggesting there has  
317 been no significant recent displacement on the eastern bounding fault (Wallace, 1977; Hodge et  
318 al., 2020).

319           In contrast, the western bounding scarp is less pronounced, and more irregular than its  
320 eastern counterpart. The elevation difference is somewhat lower too, with a maximum value  
321 between footwall crest and hanging wall cut off of c. 500 m, also located approximately midway  
322 along the fault (Fig. 5A). The scarp itself is harder to differentiate as a specific feature because of  
323 the remnant topography developed along the hanging wall (Fig. 3A). It is possible that the  
324 bounding fault is itself broken down into a number of smaller step or terrace faults, as often occurs  
325 in more asymmetric half-graben in other rift systems (e.g. Rosendahl et al., 1986; Morley et al.,  
326 1990). There are a number of transverse, tributary drainages contributing to scarp degradation, but  
327 these are less well organized and more irregularly spaced than on the eastern margin. The axial  
328 river cuts across the graben floor from the eastern to the western margin and flows for a few  
329 kilometers along the base of western scarp, locally incising into the footwall before making a  
330 junction with the Swakop River beyond the northern limit of the graben (Fig. 3A).

331           The graben floor is relatively smooth over much of its area with a gently undulating  
332 landscape, modest stream incision of a few tens of meters, and local development of what appears  
333 to be residual relief, with basement hills rising c. 100 m above the smooth graben floor. This  
334 residual topography is most clearly seen in the north of the graben, where a range of prominent  
335 hills are oriented WSW parallel to the structural grain of the bedrock and appear to continue into  
336 the footwall area on the western margin (Fig. 3A). Basement rocks are exposed over most of the  
337 graben floor, with only very localized areas where aeolian and fluvial sediment cover of a few  
338 meters thickness is preserved. The elevation of the graben floor climbs steadily towards the  
339 southern end, where the topographic expression of the graben dies out against the high ridges that  
340 cross the area in a WSW orientation and which can be linked to the major north dipping Damaran  
341 thrust quartzites mapped by Guj (1967) and Hoffmann and Schreiber (2011) (Fig. 3B).

342

## 343 **5.2. Igneous Activity**

344 As noted briefly above, there are several suites of preserved igneous bodies located within  
345 some tens of kilometers of the southern end of the Windhoek Graben, and their possible spatio-  
346 temporal connection with the development of the graben has previously been highlighted (Miller,  
347 2008). These igneous bodies are described below in four groups based on their timing and  
348 geochemical characterization, from the pioneering work of Gevers (1932, 1934), Ferreira et al.  
349 (1979), and Marsh (2010).

350

### 351 **5.2.1. The Stalhart Cluster of Phonolites**

352 The Stalhart Cluster is a group of phonolitic extrusions and/or plugs that occur over an area  
353 of 180 km<sup>2</sup> some 50 km SW of the Windhoek Graben (Fig.6) (Marsh, 2010). The Stalhart Cluster  
354 was erupted onto a highly eroded landsurface composed of Damaran quartzite (1:250,000  
355 geological map, sheet 2316). This eroded landsurface is sporadically covered by Quaternary  
356 sediments, deposited by south-flowing rivers that rise in the southern ridges of the Namibian  
357 Highlands (Fig. 6).

358 The Stalhart Cluster comprises sixteen small bodies that, in comparison with the better  
359 preserved Klinghardt phonolites, have been interpreted as eroded tholoids (Marsh, 2010). They  
360 form irregular conical hills with slightly depressed cores compared to their margins. The largest  
361 preserved body is c. 200 m high and c. 1500 m wide, but the average preserved height of the group  
362 is c.100 m with average widths of c. 1 km. The cluster was first described as a group of both  
363 phonolites and trachytes with two minor alkaline plugs (De Kock, 1934), but Marsh (2010)  
364 demonstrated from extensive sampling that, the igneous bodies are all geochemically better classed



365 as true phonolites the exception of a single minor alkaline plug. The phonolites are aphyric (<2%  
366 phenocrysts) to porphyritic (<15% phenocrysts), where the phenocrysts range from highly altered  
367 nepheline and sanidine to minor unaltered feldspathoids, followed by microphenocrysts of  
368 aegirine. More altered phonolites and steeper dips of sheeting joint and flow banding are radially  
369 concentrated in the inner core of the circular outcrops (Marsh, 2010). A fresh nepheline sample of  
370 the Stalhart cluster was dated using the  $^{40}\text{Ar}/^{39}\text{Ar}$  method, yielding a mean age of  $52.6 \pm 0.3$  Ma  
371 (Marsh et al., 2018). The associated alkaline plug is holocrystalline, porphyritic with mainly salite  
372 phenocrysts, classified as plagioclase-bearing nephelinite (Marsh, 2010), and is more weathered  
373 than the phonolites (Miller, 2008). The Stalhart phonolites and the alkaline plug have an identical  
374 initial  $^{87}\text{Sr}/^{86}\text{Sr} \approx 0.7043$  (Marsh, 2010).

375         The tholoid bodies were erupted as lava domes composed of viscous short-range flows  
376 onto the eroded basement surface (Marsh, 2010). This surface forms part of an extensive broad  
377 valley or amalgamated set of valleys whose topographic relationships to the Namibian Highlands  
378 can best be seen in a series of longitudinal and transverse profiles that we constructed with respect  
379 to the present-day valley network in this area (Fig. 6C). From the gently dipping surface on which  
380 the cluster was erupted, at an elevation of  $1580 \pm 40$  m, the surface extends smoothly northwards  
381 to the slopes of the prominent WSW Damaran quartzite ridges. Profiles ii and iv of Fig.6C, were  
382 constructed to meet the southward projection of the western footwall to the Windhoek Graben.  
383 They show that this surface (referred to here as the pre-52Myr (P52) surface) is remarkably  
384 smooth, with no significant steps or scarps over the c. 60 km distance along the connecting profiles  
385 v and vi of Fig. 6C. In contrast, the transverse profiles show a subtly concave topography in a  
386 northerly direction, with more pronounced valley forms closer to the higher topography of the  
387 quartzite ridges (Fig. 6C, profiles i to iv). Taken together, these profiles show that the P52 surface

388 can be interpreted as a preserved valley or valley system with generally south-flowing axes, and  
389 at whose southern end the Stalhart Cluster was erupted (Fig. 6A). This implies that significant  
390 incision of some hundreds of metres magnitude must have been carved by the south-flowing rivers  
391 prior to eruption of the Stalharts. This interpretation thus completely endorses the view of (Marsh,  
392 2010) that the lava domes were emplaced onto a surface not very different in its relief from the  
393 present-day surface and have been eroded down to expose the upper parts of the conduits where  
394 the steeper dips of flow banding and sheeting joints toward the core areas can be seen exposed  
395 today.

396

### 397 **5.2.2. The Aris Cluster of Phonolites/Trachytes**

398 The Aris Cluster is located ~15 km south of the Windhoek Graben close to the head of the  
399 Usib Valley, at an elevation of 1770 m  $\pm$  30 m (Fig. 6 and 7A). The Aris Cluster comprises six  
400 individual phonolite bodies (Marsh, 2010), about five smaller bodies of trachyte, and a small body  
401 of trachyte breccia (Miller, 2008). Of these, the two largest bodies are Schildkrotenberg and  
402 Huguamis, composed of phonolite, and forming strikingly conical hills, and partially dissected by  
403 the south-flowing Usib River (Fig. 7A-C). Schildkrotenberg rises 290 m above the valley floor  
404 and is 1900 m wide at its base.

405 Topographic profiles between the Stalhart and Aris Clusters demonstrate that the elevation  
406 of the Aris Cluster is about 200 m higher up and further up the valley relative to the Stalhart cluster  
407 and is surrounded by highly dissected terrain on three sides (Fig. 6A and C). The head of the Usib  
408 River occurs 5 km north of the cluster, where a WSW striking ridge of quartzite acts as a drainage  
409 divide between the Windhoek Graben in the north and the Usib Valley in the south. The  
410 morphology of the Usib Valley opens up to the south, from the narrow valley onto which the Aris

411 Cluster was erupted to the more laterally extensive surface onto which the Stalharts were erupted.  
412 The valley is predominantly cut into pre-Damaran paragneiss and this basement is locally covered  
413 by a thin veneer of Quaternary sediments (Fig. 7B and 7C) (1:250,000 geological map, sheet 2216).

414 The nature of the phonolite outcrops (e.g., morphological shape, degree of weathering, and  
415 structural trend) is identical with the Stalhart phonolites (Marsh, 2010). The phonolites are  
416 holocrystalline fine- to medium-grained, mainly aphyric to lightly porphyritic with insignificant  
417 trachytic textures (Miller, 2008; Marsh, 2010). The groundmass of both aphyric and porphyritic  
418 phonolites is dominated by nepheline and sanidine (Marsh, 2010). The Aris phonolite composition  
419 is marked by a more homogeneous concentration of trace elements with generally lower TiO<sub>2</sub>, Sr,  
420 Nb, and higher Na<sub>2</sub>O, Rb, Zr, Th, Pb, and REE compared to the Stalhart phonolites (Marsh, 2010).  
421 One phonolite body was dated using a whole-rock <sup>40</sup>Ar/<sup>39</sup>Ar method and generated an age of 32 ±  
422 0.2 Ma (Burger and Walraven, 1976). This date has been questioned as to its accuracy by Marsh  
423 et al. (2018), who noted that the whole rock method generally lacks precision in comparison to  
424 more modern single grain techniques and suggests from comparisons in the ages of the Klinghardt  
425 Mountains that this date could easily be in error by up to 10 Ma.

426 The trachytes and trachyte breccia are not as extensively described as the phonolites, and  
427 their bodies are ~10 to 30% smaller than the size of the biggest phonolite (i.e., Schildkrotenberg).  
428 The formers appear as plug-like features and are mainly made of massive, chemically altered  
429 trachytes, tuffaceous trachyte, and breccia containing gneiss fragments along the margins of the  
430 body (Miller, 2008; Marsh, 2010). The latter forms a pipe-like feature and consists of trachyte  
431 breccia containing abundant xenoliths (e.g., gneiss and quartz) (Niku Paavola, 1997; Miller, 2008).

432 Marsh (2010) interpreted the Aris phonolites as eroded tholoids based on their  
433 morphological and petrological character, similarity to the Stalhart phonolites, and argued that

434 they were also emplaced on a surface not very different in its relief from the present-day surface  
435 (PDS) (Fig.7D). Higher Rb, Zr, Th, Pb, REE, but lower Sr, Nb, and narrow compositional range  
436 for the trace elements indicate that the Aris phonolites were highly evolved and originated from a  
437 single magma system (Marsh, 2010). The close proximity of the bodies of trachyte and breccia are  
438 then postulated as associated members during the emplacement of mafic magmas to the surface.  
439 However, the magmatism of the Aris cluster was different from the Stalhart cluster as Aris  
440 phonolites are younger, morphologically less eroded, and geochemically more homogeneous than  
441 the Stalhart phonolites (Marsh, 2010).

442 Combining all the observations with the topographic profiles, we conclude that the valley  
443 erosion that pre-dated the eruption of the Stalhart Cluster and formed the pre-52Myr surface was  
444 not obviously modified by further erosion prior to the eruption of the Aris Cluster in the Oligocene  
445 (Fig. 7D). Considering that there has been relatively limited subsequent erosion of the tholoids  
446 bodies of the Aris Cluster, we also conclude that the Usib Valley was largely formed in its present  
447 configuration by the Early Eocene (i.e., prior to 52 Ma).

448

### 449 **5.2.3. The Regenstein Vent Complex**

450 The Regenstein vent complex is situated west of the southern end of the Windhoek Graben  
451 (Fig.6A). It differs in its topographic position from the Aris and Stalhart Clusters in that it forms  
452 an erosional depression within one of the prominent SW ridges of Damaran quartzite (Ferreira et  
453 al., 1979), with an average elevation of 2080 m or ~300 m above the valley floor location of the  
454 Aris cluster (Fig. 7C). This ridge is cut by the head of the Usib Valley at c.1900 m asl before it  
455 climbs to the far northeast of the Regenstein complex, reaching up to 2465 m asl, with an average  
456 peak elevation of about 2400 m over a 15 km length (Auas Mountains, Fig. 7A).

457           The outcrop of the irregular-shaped vent mostly occupies low ground, but the contact with  
458 the basement, quartzites can be traced over some 160 m of vertical relief, up to an elevation of  
459 2120 m (Gevers, 1934) (Fig. 8). These basement quartzites have been found to be important  
460 aquifers in the region surrounding Windhoek (Miller et al., 2018). The vent complex consists of  
461 the main body with a length of 2 km and width of 1 km in an elliptical shape trending NNW-SSE  
462 and an isolated, smaller associated body located 500 m to the north (Gevers, 1934; Ferreira et al.,  
463 1979). The area is heavily faulted (Gevers, 1934). A set of NNW-SSE striking faults occur at the  
464 western margin of the vent complex, extending from the northern satellite body to the main body  
465 in the south (Ferreira et al., 1979). The faults are marked at outcrop by silicified, brecciated shear  
466 zones and the most prominent of these (Fig. 9A) runs from the center of the main body to the  
467 northern satellite body (Ferreira et al., 1979).

468           The Regenstein vent complex comprises distinct bodies of mainly pyroclastic breccia and  
469 marginally mafic rocks and dykes (Ferreira et al., 1979), and has not been radiometrically dated,  
470 presumably because of the high degree of hydrothermal alteration of the vent materials. The  
471 breccia is composed of fragments of highly-altered accidental clasts (mainly quartzite) and  
472 accessory clasts (phonolites, trachytes, and lapilli breccia) with clay minerals and carbonate  
473 cement ranging in diameter from 2 mm to 0.5 m. The trachytic-quartzite breccia is predominantly  
474 observed in the in the low lying outcrop areas of both vent bodies (Ferreira et al., 1979; Miller,  
475 2008). Marginal bodies of fluidised quartzite breccia are found discontinuously along the western  
476 edge of the vents with a sharp contact with the surrounding highly-fractured Damaran quartzite.  
477 Radial fractures from the center of the vent cut through these two rock types and are filled by  
478 fluidized, well rounded quartzite fragments, testifying to the explosive nature of the eruptions  
479 resulting in the vent structure (Miller, 2008). The distribution of these pyroclastic breccias has

480 been extended ~200 m below the present-day surface based on an exploratory borehole in the  
481 northeastern area (Ferreira et al., 1979).

482 A noticeable mafic body forms an irregular conical hill with a diameter of 250 m in the  
483 northwestern area of the main vent, and its location is spatially aligned with the NNW-SSE  
484 trending fault. It is composed of heterogeneous mafic phonolites showing the medium-grained,  
485 hypidiomorphic-granular texture of mafic xenoliths enclosed in a fine-grained, porphyritic matrix  
486 (Ferreira et al., 1979; Miller, 2008). Dykes are thin and radiate from the center of the vent,  
487 demonstrating a sharp contact with the breccias (Gevers, 1934; Ferreira et al., 1979). These dykes  
488 are composed of phonolite, biotite trachyte, and aegirine trachyte. The trachyte dykes cut through  
489 the dykes of phonolites (Miller, 2008, and references therein).

490 Emplacement of the Regenstein vent complex has been interpreted to be phreatomagmatic  
491 in repetitive cycles, and its location is thought to be structurally controlled (Ferreira et al., 1979).  
492 The interpretation of the eruptive mechanism and cyclic emplacement history is supported by an  
493 absence of essential elements in the breccias, by the silicified fault zones, by fracturing and  
494 fragmentation of the marginal quartzite, by hydrothermal alteration, and by the various textures of  
495 the pyroclastic breccias (e.g., trachyte and phonolites). Structural control is corroborated by the  
496 shape of the main vent in relation to an important cluster of normal faults identified by Ferreira et  
497 al. (1979) (Fig. 3B). This cluster of normal faults coincides approximately with the longest axis  
498 of the vent complex and the locations of the mafic body, and an anomalous trend of Pb-Zn  
499 mineralisation (Ferreira et al., 1979). Ferreira et al. (1979) proposed that the breccia was first  
500 emplaced with the phonolite and trachyte dykes, followed by the emplacement of mafic rocks that  
501 were finally altered by hydrothermal processes.

502           The vent complex thus represents a deeper conduit system that has been exhumed due to  
503 erosion of a land surface that existed at the time of its emplacement. From their detailed mapping,  
504 Ferreira et al. (1979) argued that this palaeo-surface was about 400 m above the present erosion  
505 level of the main vent structure (Fig. 7D). Topographic profiles from the Regenstein Vent Complex  
506 to the Aris and Stalhart Clusters demonstrate that this palaeo-surface (referred to as a pre-  
507 Regenstein surface (PRS)) onto which the phreatomagmatic products erupted, possibly as a maar-  
508 like pyroclastic cone, could not have been a continuation of the pre-52Myr surface (P52), but must  
509 instead have been at a higher level by several hundred meters (Fig. 7D). This is entirely consistent  
510 with Gevers's (1934) view that the Regenstein Vent is Late Cretaceous in age and significantly  
511 older than the Aris Cluster.

512

#### 513 **5.2.4. Dykes, Plugs, and Brecciated Fissures of the Southern Windhoek Graben area**

514           Dykes and elongated plug-like intrusions mainly of trachyte were mapped in great detail  
515 by Gevers (1932) and Guj (1967). They found more than 160 individual intrusive bodies that are  
516 distributed mainly in the southern limit of the Windhoek Graben and in the vicinity of the WSW  
517 trending quartzite ridge (Fig. 6A). The longest dyke in this area is 12 km, and the average thickness  
518 is less than 10 m (Gevers, 1932; Miller, 2008). The dykes are almost vertical, dipping generally  
519 75° to 80° in the southern Windhoek Graben area (Gevers, 1932). In the southeastern region of the  
520 major WSW trending quartzite ridge, the width of individual trachyte intrusions may reach up to  
521 200 m and these are generally porphyritic in texture with vertical contacts with the basement rocks  
522 (Guj, 1967; Miller, 2008). Individual trachyte dykes intersect the crest of the ridge at an altitude  
523 of c. 2300 m, and their contacts can be traced down to c. 1900 m, implying that several hundred  
524 metres of erosion has taken place post-emplacement. In order to compare the orientation of these

525 dykes and plugs with the orientation of minor normal faults in the southern area of the Windhoek  
526 Graben, we also measured the mapped strikes of 162 linear trachyte plugs and dykes using  
527 compilations of Gevers (1932) and Guj (1967). Their orientations range from NW to NNE strikes  
528 (Fig. 6B), and notably, this range of strikes compares very well with the strikes of the minor normal  
529 faults mapped in the southern Windhoek Graben (Fig.5D).

530         The dykes are predominantly trachytic and phonolitic in composition and extend from the  
531 center of small vents, and from trachyte and breccia plugs (Gevers, 1932). Sets of dykes cut across  
532 the Damaran thrust faults on the major WSW trending ridge while other groups of dykes terminate  
533 at thicker quartzite units juxtaposed across the thrust faults (Gevers, 1932; Miller, 2008). Most of  
534 the dykes are highly brecciated and are associated with siliceous impregnation zones and fissures  
535 that were brecciated and filled by siliceous material (Gevers, 1932). The dykes appear inside the  
536 core, alongside, or as an extension of the silicified fault zones in the southern Windhoek Graben  
537 and also cluster together as a dyke swarm between two sets of northerly striking normal faults  
538 (Miller, 2008). Only a few dykes cut across the silicified fault zones at a high angle (Miller, 2008).  
539 The silicified breccia dykes generally exhibit displacements of less than a few meters along their  
540 strike, but groups of fissures are both longer and wider along both margins of the southern  
541 Windhoek Graben (Gevers, 1932). Thermal springs are associated with the brecciated fissures,  
542 with the highest temperature reaching up to 79.8°C in the eastern margin area of the southern  
543 Windhoek Graben (i.e., Pahl Spring) (Gevers, 1932).

544         The geometry, distribution and composition of the dykes and brecciated fissures (breccia  
545 dykes) have been taken by (Gevers, 1932; Miller, 2008) to argue that they were emplaced during  
546 intense phreatic-fumarolic activities and were spatially and temporally associated with the small  
547 vents, trachyte plugs, and the minor faults of the southern Windhoek Graben. Given that the



548 orientations (and in some cases locations) of dykes generally correspond to the strikes of the minor  
549 normal faults in the southern area of the Windhoek Graben (Fig. 5D and Fig. 6B), this points to a  
550 direct link between the normal faulting with a generally E-W extension direction and this phase of  
551 igneous activity.

552

## 553 **6. DISCUSSION**

554 Two main questions arise from the preceding summary of the observations regarding the  
555 southernmost faults of the Windhoek Graben and the four sites of igneous activity, namely:

556 (1) What is the precise relationship between the broad swathe of normal faulting mapped  
557 in the area of the southern Windhoek Graben, the abundant trachyte and breccia dykes distributed  
558 along the major quartzite ridge, foothills, and the Regenstein Vent Complex?

559 (2) How can the topographic relationships between the various igneous centers be used to  
560 build a chronological framework for the initiation of the Windhoek Graben?

561

### 562 **6.1. The Windhoek Graben and Its Relationship to the Regenstein Vent Complex**

563 Based on the relationships between igneous bodies and normal faults (Fig. 9), we suggest  
564 that the southern limit of the Windhoek Graben abuts and terminates against the WSW trending  
565 quartzite ridge on which the Regenstein Vent Complex is situated. We furthermore argue that the  
566 graben initiated in the same time interval as the igneous activity that resulted in the Regenstein  
567 Vent Complex and the cluster of trachytes dykes, breccia dykes, and trachyte plugs and vents in  
568 this area (Fig. 9). Three main arguments favour this interpretation.

569 Firstly, normal faulting that is clearly linked to the development of the southern region of  
570 the Windhoek Graben is demonstrably spatially and temporally linked to the emplacement of the

571 Regenstein Vent Complex through the propagation of the graben-margin faults and smaller faults  
572 that displace the phreatomagmatic breccia dykes (Gevers, 1932; Ferreira et al., 1979). We  
573 essentially follow the interpretation of Miller (2008), who proposed that the west bounding fault  
574 of the Regenstein Vent Complex runs continuously to the Swakop River in the north (Fig. 3A).

575 Secondly, the common phreatomagmatic nature of the Regenstein Vent Complex and the  
576 trachyte dykes is a strong argument to support Gevers' (1932) arguments linking these suites of  
577 intrusive bodies. It seems unlikely that such a large number of spatially clustered phreatomagmatic  
578 products and silicified fault zones would be linked purely coincidentally. Therefore, these  
579 observations collectively argue that the initiation of the Windhoek Graben is spatially and temporal  
580 related to the igneous activity centred on the Regenstein Vent Complex.

581 Finally, the strikes of the >100 normal faults distributed in this southern terminus region  
582 of the Windhoek Graben have a closely comparable distribution to the strikes of the >160 dykes  
583 in the same area (Fig. 5D and 6B). Both sets of structures evidently developed in a very similar  
584 stress field, in both cases with the minimum compressive stress horizontal and oriented E-W. The  
585 simplest interpretation of this uniformity of the driving stress state for dykes and faults is that the  
586 normal faulting occurred during the same tectonic episode as the dyke intrusion. Since the dykes  
587 are linked in time and also partly spatially to the Regenstein Vent Complex, we argue that the  
588 initiation of normal faulting was also most probably linked to this igneous event. This  
589 interpretation is favoured over the alternative view that the faulting and dyke formation are  
590 completely unrelated, because the normal faults do not systematically offset the dykes, and neither  
591 do the dykes cross-cut the normal faults.

592

## 593 **6.2. Chronological Framework for the Initiation of the Windhoek Graben**

594 From the preceding arguments, we suggest that we can constrain the timing of initiation of  
595 the Windhoek Graben by placing the emplacement of the Regenstein Vent Complex into a  
596 chronological framework based on the correlation of remnant erosional surfaces.

597 The reference datum for our proposed chronological framework is defined here as the  
598 surface onto which the eruptive products from the Regenstein Vent were emplaced. Ferreira et al.  
599 (1979) estimate that the palaeo-surface intersected by the vent at the time of eruption was c.400 m  
600 above the height of the current topographic depression (Fig. 9C). They based this estimate on  
601 consideration of mapped contact morphology, drilling results and vent fill characteristics,  
602 recognizing that considerable erosion of c. 400m of the vent has occurred since emplacement.  
603 Trachyte dykes within the basement are mapped at similar elevations further east along the major  
604 quartzite ridge as shown in (Fig 7B and 9A). Making the assumption that these trachyte dykes  
605 were intruded with their upper tips close to the palaeo-surface, then we can interpolate between  
606 these two positions on the ridge to identify a conservative position for this palaeo-surface, which  
607 we refer to here as the pre-Regenstein surface, PRS (Fig. 7D and 9C).

608 To place any form of absolute age constraint on this surface requires long-range correlation  
609 and large assumptions in making that correlation. However, previous workers have been struck by  
610 the accordance of many of the local summits of the series of ridges that stand above the plains and  
611 valleys of the broad area flanking the Aranos Basin and the Namibian Highlands (e.g., Fig. 4C and  
612 Fig. 6C (iii, vi, viii)). Gevers (1942) argued that the accordant summit heights of the ridges must  
613 represent the remnant of a higher, older surface that forms an envelope to the present-day  
614 topography of the Namibian Highlands. He also described a spectacular example of superimposed  
615 drainage in this area, where the Usib River cuts through one of the more distal ridges (Fig. 10). He  
616 argued from the cleft in the ridge cut by the river down to its present-day level, that there must

617 have been a gently inclined surface at or above the level of the present-day ridge crest in order for  
618 the river to cut down through the ridge rather than circumnavigate around the ridge. This surface  
619 on which the ancestral Usib evidently flowed southwards was most probably the pre-Regenstein  
620 surface (PRS), since it conforms to the simple interpolation of ridge summit heights shown in Fig.  
621 10C and D.

622         Correlation of this pre-Regenstein surface (PRS) southwards from the major quartzite ridge  
623 gives a notional impression of a relatively planar older surface, but how does this surface correlate  
624 into regions of subsurface chronostratigraphic control? The closest outcrops of Mesozoic  
625 sedimentary rocks to the data point at the Usib Gorge are close to Mariental, some 150 km to the  
626 south. Projection of the PRS could justifiably be made with additional examples of superimposed  
627 drainage on some of the more distal ridges (Fig. 10B and D) and this closes the gap to less than 50  
628 km. However, an even more well-constrained projection can be made into the subsurface of the  
629 Aranos Basin using water boreholes as the primary data points for key surfaces (Fig. 11). These  
630 boreholes calibrate the base of the Kalahari Group sediments (interpreted as Late Cretaceous in  
631 age; Miller, 2008) and also the Base of the Karoo Supergroup. The projection along this section  
632 shows that the PRS projects close to the convergence of three major unconformities, namely the  
633 Base Nama Group, Base Karoo, and Base Kalahari. We can reasonably rule out the Base Nama as  
634 being the progenitor of the PRS on the basis that it dates from the Late Precambrian to Cambrian.  
635 This leaves us with the more reasonable interpretation that the PRS is the lateral correlative of a  
636 compound unconformity surface of these two other major unconformities, i.e., a pre-Karoo surface  
637 modified by events leading into the latest Cretaceous/earliest Cenozoic. By correlation with the  
638 regional cross-sections presented by Picart et al. (2020), our PRS corresponds to their oldest  
639 surface, S0, but they did not provide a date for the formation of this surface. Similarly, we correlate

640 our P52 surface as being approximately equivalent to the undated surfaces S1 and S2 of Picart et  
641 al. (2020).

642         The questions arising from this interpretation of the PRS are firstly, is there any  
643 independent support for this notional correlation, and if so, what does it imply about relative uplift  
644 of the Namibian Highlands with respect to the neighbouring areas? The interpretation that the pre-  
645 Regenstein surface (PRS) is a Late Cretaceous to Early Cenozoic modified remnant of a pre-Karoo  
646 surface is strongly supported by evidence of deep incision of the Karoo Supergroup sediments  
647 within the Aranos Basin, as documented by Miller (2008). Correlation of lateritic alteration of the  
648 incised Karoo clastic sediments led Miller (2008) to the conclusion that a south-eastward flowing  
649 river, which he termed the Aranos River, originated in the Late Cretaceous. His argument is based  
650 on meticulous comparison of depths to the top of the lateritized Karoo in water boreholes, and the  
651 preserved thickness of the laterite layer. This demonstrated that the fluvial incision occurred during  
652 the humid climatic conditions required for the development of the laterite profile, which from  
653 regional considerations he placed in the latest Cretaceous to earliest Cenozoic. He also noted that  
654 this incision most likely coincided with the onset of subsidence in the Aranos Basin, which is  
655 widely regarded as Late Cretaceous in age (Partridge and Maud, 1987; Moore, 1999). It seems  
656 entirely plausible that this Late Cretaceous origin of the Aranos River was replicated for  
657 neighbouring major drainages, including that responsible for the erosion of the Usib Valley, which  
658 we have already argued must have been almost completely incised close to its present-day profile  
659 by 52 Ma.

660         Extending this logic to the wider context of the Namibian Highlands, therefore, leads us to  
661 conclude that the most likely period for onset of valley development on the eastern and southern  
662 flanks of the highlands was during the Late Cretaceous. Evidence for the timing of initiation of the

663 westerly flowing rivers like the Kuiseb and the Swakop (see Fig. 2A) is lacking at present, but  
664 Clemson et al. (1997) and Aizawa et al. (2000) both noted the development of incised valleys in  
665 the offshore corresponding to the modern river outlets, that were clearly cut within the latest  
666 Cretaceous. This would strongly suggest that well-established rivers were flowing across the site  
667 of the Great Escarpment at this time, and were probably rising on the western flank of the Namibian  
668 Highlands. If correct, this would in turn suggest that the Namibian Highlands were the locus of a  
669 radial drainage pattern dating from this time, and point to a period of pronounced doming of the  
670 pre-Regenstein surface (PRS) at this time. Similarly, Raab et al. (2002) argued from their analysis  
671 of the denudational history of central Namibia using fission track data that the major erosion and  
672 sediment transport into the offshore took place between 80Ma and 60Ma. It is not possible to be  
673 more precise in the timing, but we note that numerous previous studies have argued for a  
674 significant period of uplift of the area further south towards the Orange River in the Late  
675 Cretaceous either from Low T thermochronology or from studies of the sediment transport into  
676 the offshore basins (Aizawa et al., 2000; Jacob, 2005; Bluck et al., 2007; De Wit, 2007; Baby et  
677 al., 2020; Wildman et al., 2021).

678 In conclusion therefore, the evidence assembled here points to a major phase of domal  
679 uplift of the Namibian Highlands in the Late Cretaceous. This overlapped with or was coeval with  
680 the emplacement of Regenstein Vent Complex and associated trachyte dykes and hydrothermal  
681 system, and critically, with the initial fault growth of the Windhoek Graben. Based on this, it is  
682 possible to view the origins of rifting in this area as part of a geodynamic context that considerably  
683 precedes the much more recent propagation of the Central African Rift System (Daly et al. 2020),  
684 but we cannot exclude the possibility of much more recent activity of the Windhoek Graben linked  
685 to westward propagation of this younger rift system.

686           It is tempting to speculate that the magmatic event, the uplift, and the graben initiation are  
687 all linked to wider events along the borderlands between the continental margin and the continental  
688 interior, that completely transformed the drainage development in the greater Namibian region.  
689 Understanding these events in the broader context of the geodynamic evolution of Southern Africa  
690 should ultimately lead to a fuller understanding of why the Windhoek Graben developed at this  
691 time and in this place.

692

## 693 **7. CONCLUSIONS**

- 694 1. The initiation of rifting of the Windhoek Graben is most probably related in timing to the  
695 emplacement of the Regenstein Vent Complex and its associated suite of dykes and  
696 phreatomagmatic trachyte vein and breccia dykes.
- 697 2. Morphological correlations clearly establish that previous suggestions that the vent complex  
698 predated the eruption of the Stalhart Cluster are correct.
- 699 3. Correlation of a reconstructed palaeo-surface (PRS) with deep erosion and regolith formation  
700 in the nearby Aranos Basin gives a most likely timing of Late Cretaceous to Early Cenozoic  
701 for Regenstein and the associated trachyte dyke cluster, and this can be no younger than the  
702 52-Ma date for the Stalhart Cluster.
- 703 4. The initiation of rifting is interpreted to coincide with the initial phase of magmatic activity in  
704 the area in the Late Cretaceous to Early Cenozoic.
- 705 5. The initiation of rifting was closely linked in timing to the formation of a localized domal  
706 uplift, responsible for the development of a radial drainage network that has persisted, albeit  
707 intermittently with climatic variations to the present day.

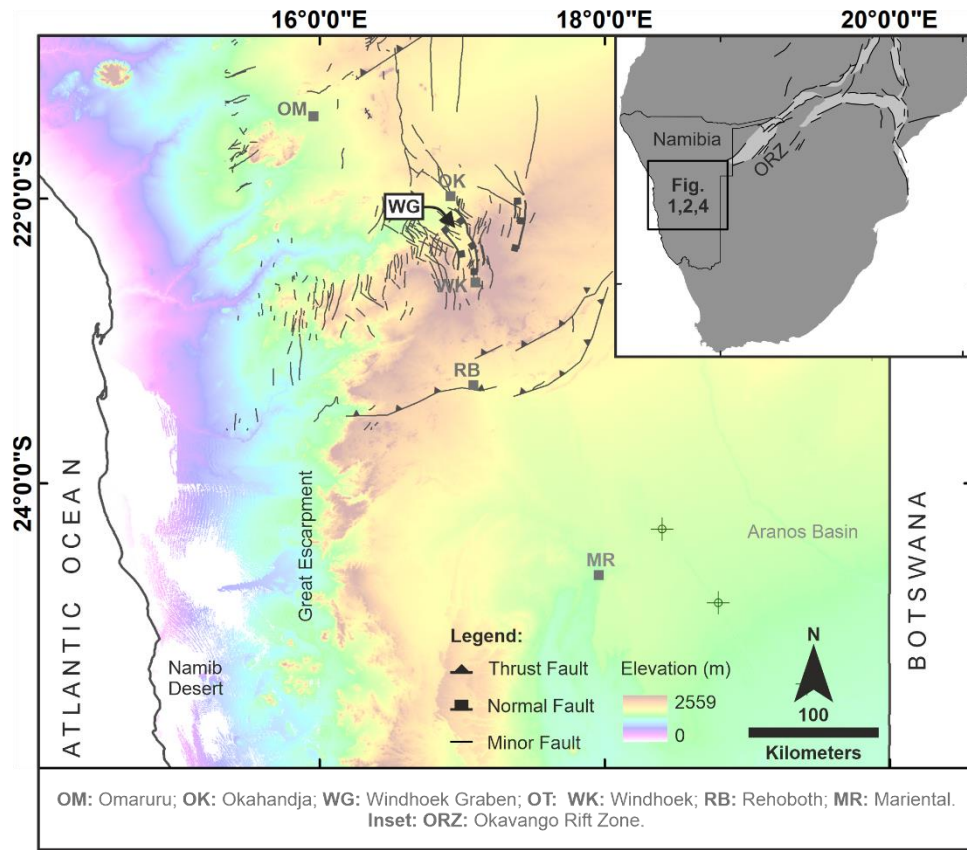
708

709 **ACKNOWLEDGEMENT**

710 This paper is part of DPhil research of RW. The authors thank Indonesia Endowment Fund for  
 711 Education (LPDP/201908223015114) for funding RW. We are grateful to CASP for awarding an  
 712 Andrew Whitham Fieldwork Award to support RW fieldwork. We thank the Geological Survey  
 713 of Namibia for providing digital copies of geological maps. Branko Corner and Karl Hartmann are  
 714 thanked for their perspectives on Windhoek Graben.

715

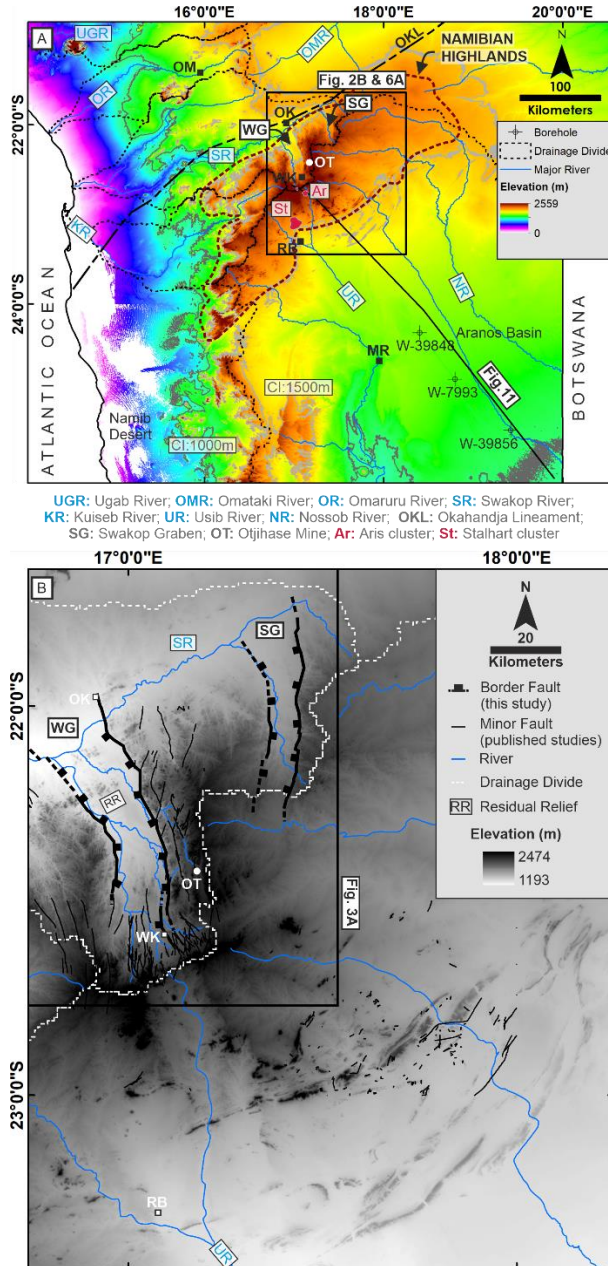
716 **FIGURES**



717

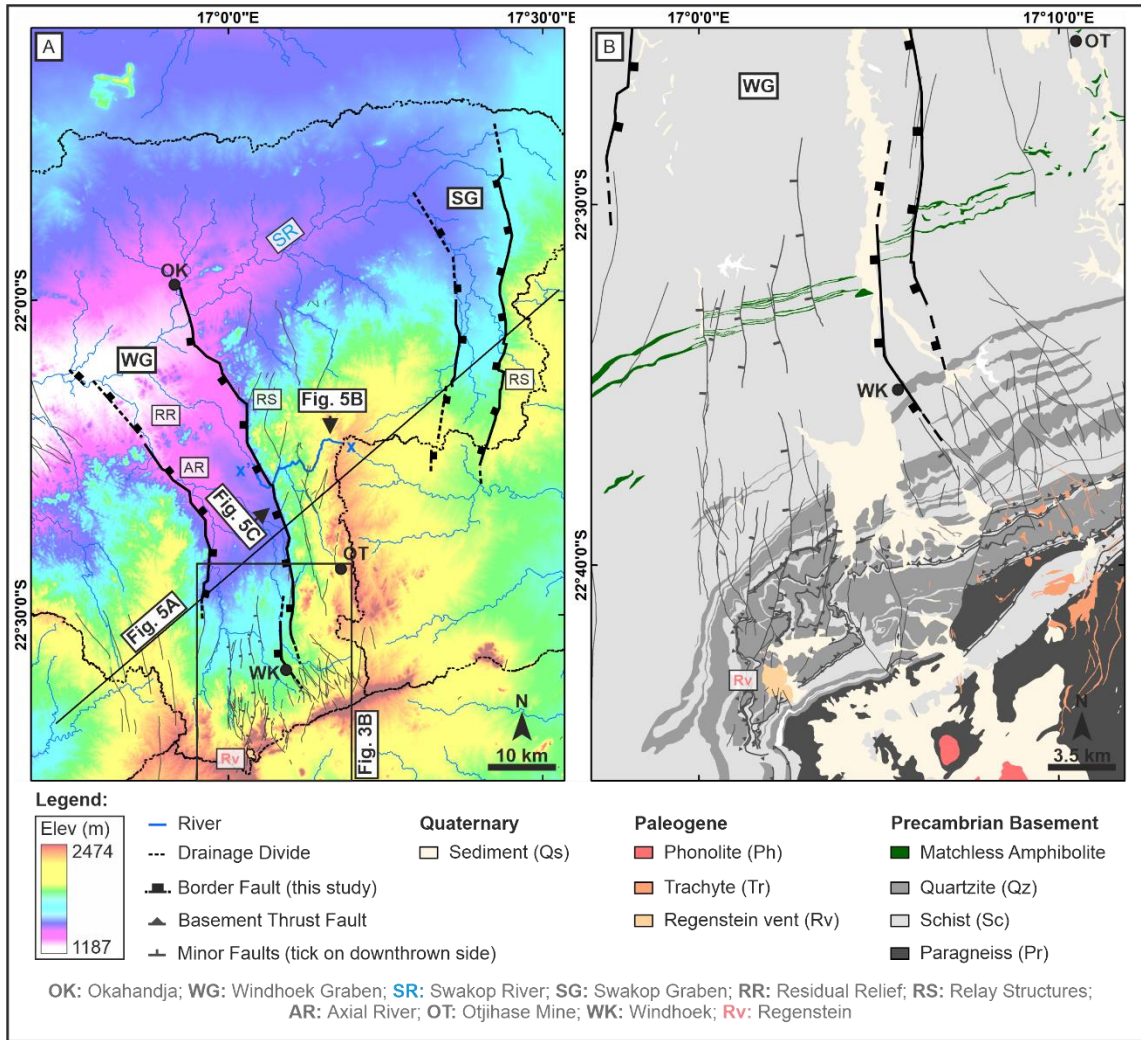
718 **Figure 1.** Regional topographic map of the study area in central Namibia overlain by a compilation  
 719 of structural maps by Guj (1967), Miller and Schalk (1980), and Picart et al. (2020). Inset: Rift  
 720 system in southern Africa (simplified from Morley et al. (1990), Kinabo et al. (2007), Ponte et al.  
 721 (2019), and Daly et al. (2020)) and Namibia location.





722

723 **Figure 2.** (A) The physiographic context of central Namibia showing Windhoek Graben (WG)  
 724 and Swakop Graben (SG) at the center area and the Aranos Basin to the south. Representative  
 725 boreholes are taken from Miller (2008). (B) Fault interpretation of Windhoek and Swakop Grabens  
 726 is superimposed on the topographic map. Minor faults are taken from Hoffmann and Schreiber  
 727 (2011) for Windhoek area and Miller and Schalk (1980) for regional area. Dip direction of the  
 728 minor faults in southern Windhoek is adapted from Miller et al. (2018). Abbreviations are in (A).



729

730 **Figure 3. (A)** Topographic map overlain by a structural map of the Windhoek Graben showing

731 outcropping segmented, curvilinear normal faults and prominent escarpments along the footwall.

732 Minor faults are taken from Hoffmann and Schreiber (2011) for Windhoek area and Miller and

733 Schalk (1980) for regional area. Dip direction of the minor faults in southern Windhoek is adapted

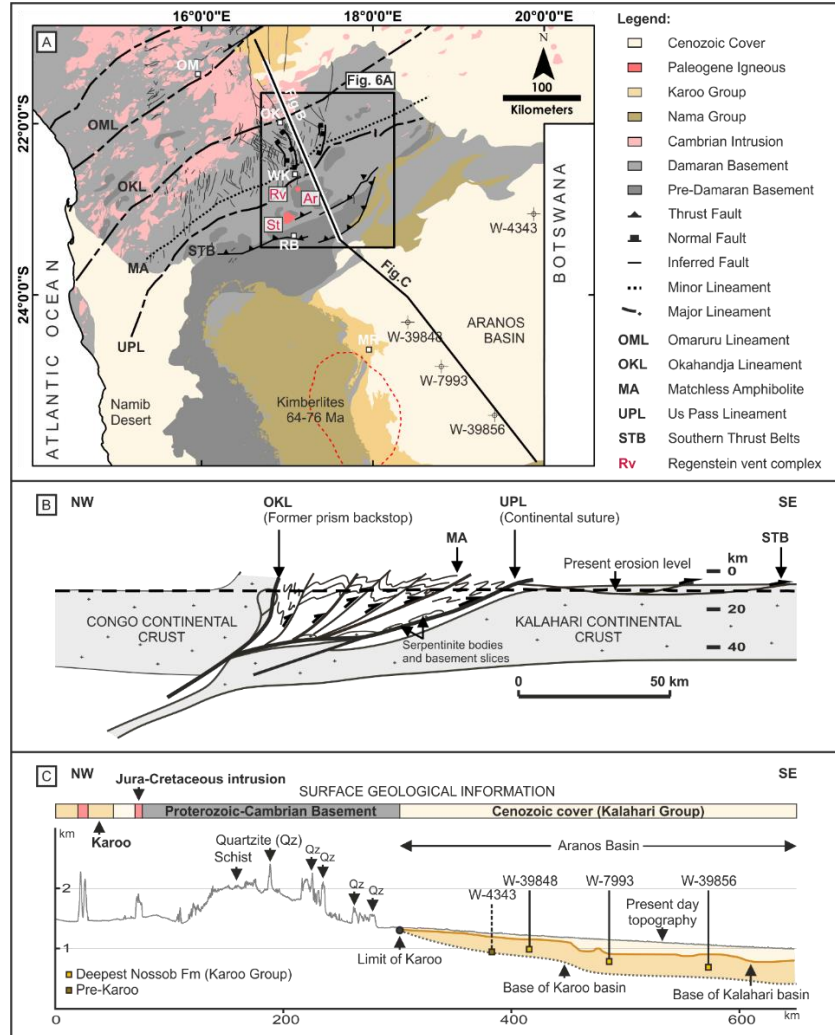
734 from Miller et al. (2018). Note: Regenstein vent complex (Rv) is located to the southwest of

735 Windhoek city (digitized from Hoffmann and Schreiber (2011)). **(B)** 1:250,000 geological map of

736 the area (sheet 2216, Geological Survey of Namibia) showing southern area of the Windhoek

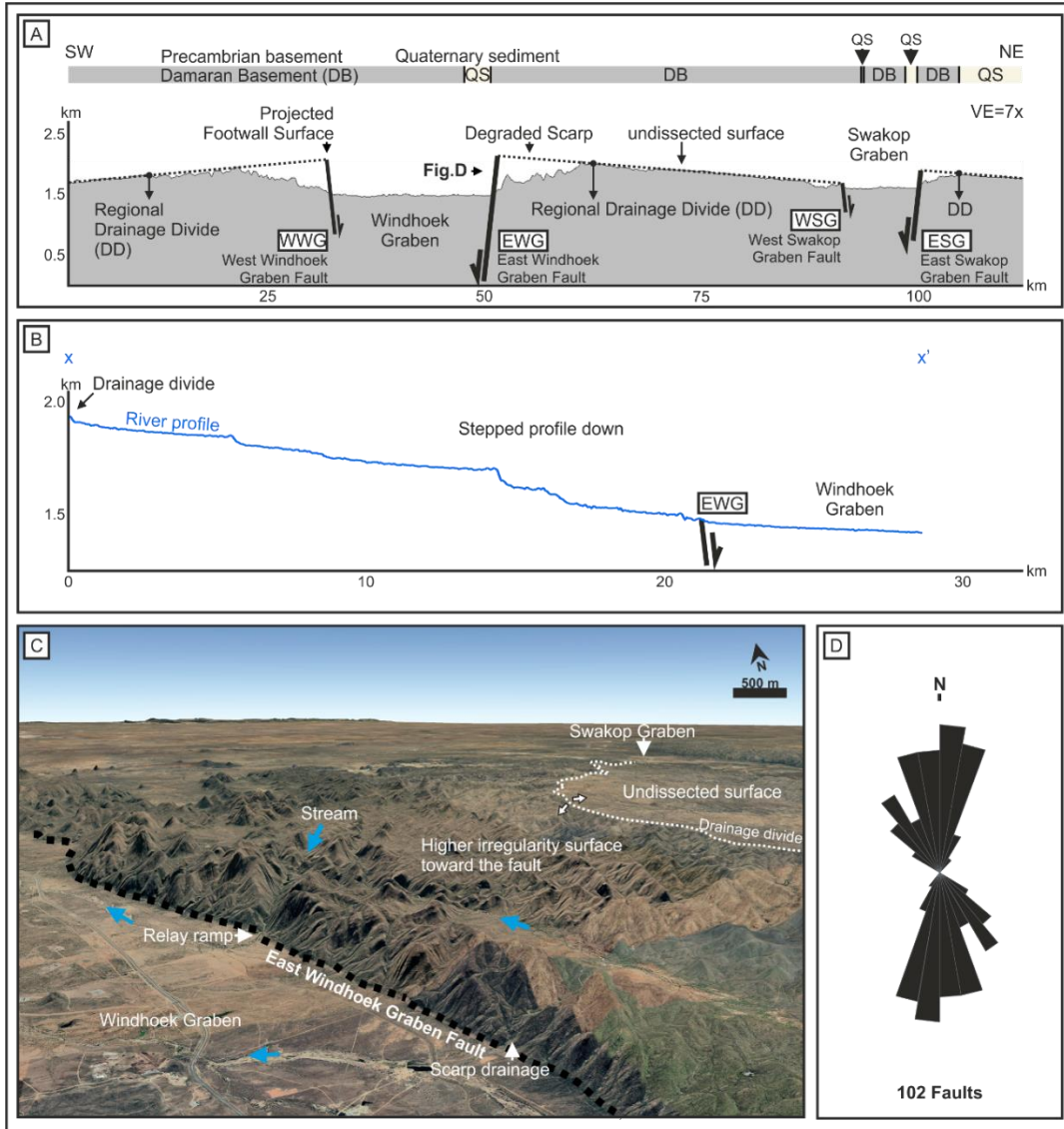
737 Graben. See (A) for location.

738



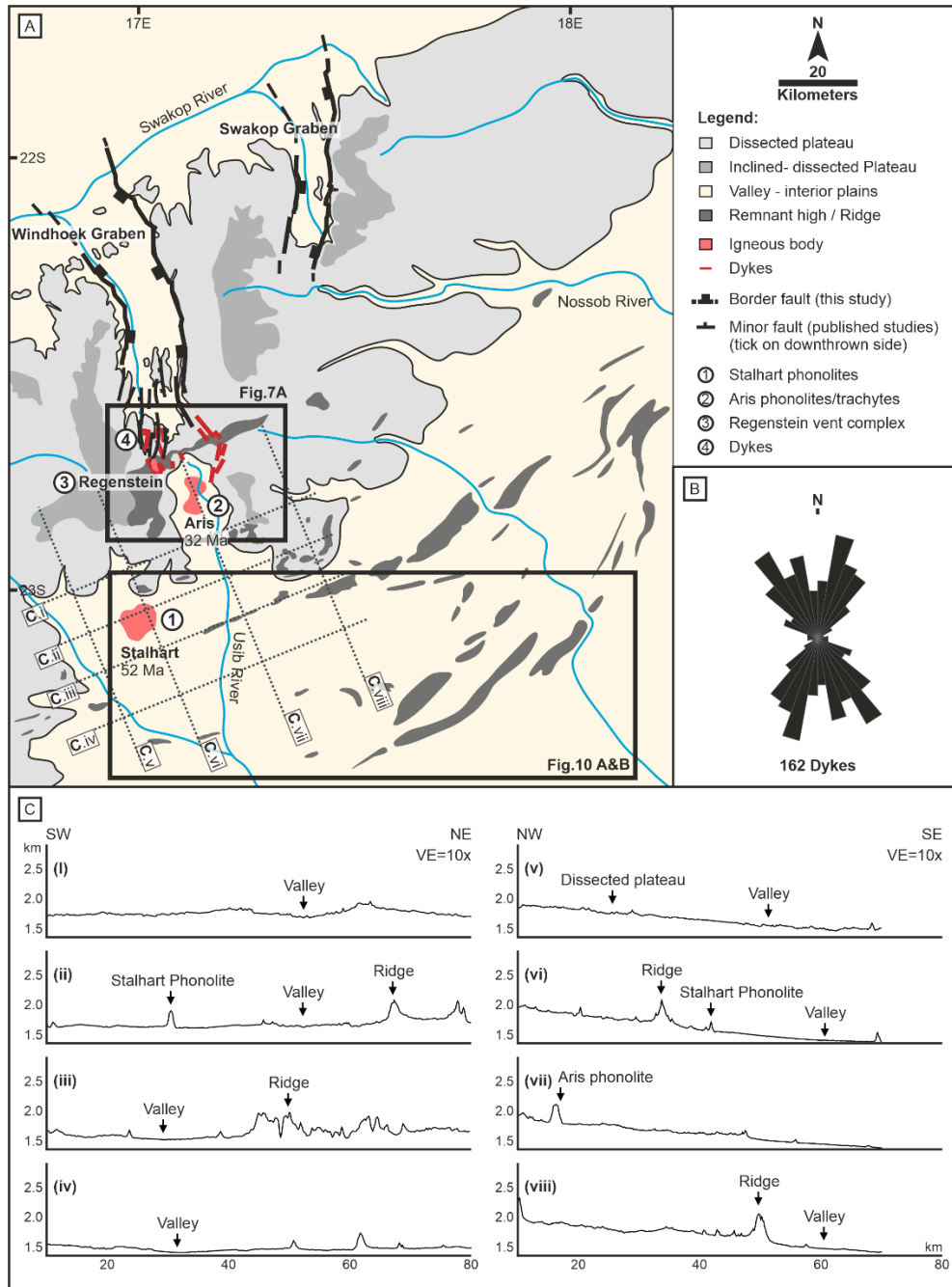
739

740 **Figure 4.** (A) Tectonostratigraphic zones of Damaran orogenic belt (modified from Hoffmann  
 741 (1983), Miller (1983), and Miller and Schalk (1980)) overlain by Nama and Karoo Groups (Miller  
 742 and Schalk, 1980), igneous bodies (Burger and Walraven, 1976; Moore et al., 2008; Marsh, 2010),  
 743 N-S grabens (digitized from Picart et al., 2020), and Cenozoic cover (Miller, 2008). Representative  
 744 boreholes are taken from Miller (2008). (B) NW-SE cross-section illustrates crustal-scale  
 745 architecture (adapted from Kasch, 1986; Kukla, 1992). (C) Regional NW-SE topographical profile  
 746 depicts morphology and surface geological information of the study area. The Aranos basin-filled  
 747 architecture is derived from Miller (2008). See panel (A) for locations of (B) and (C).



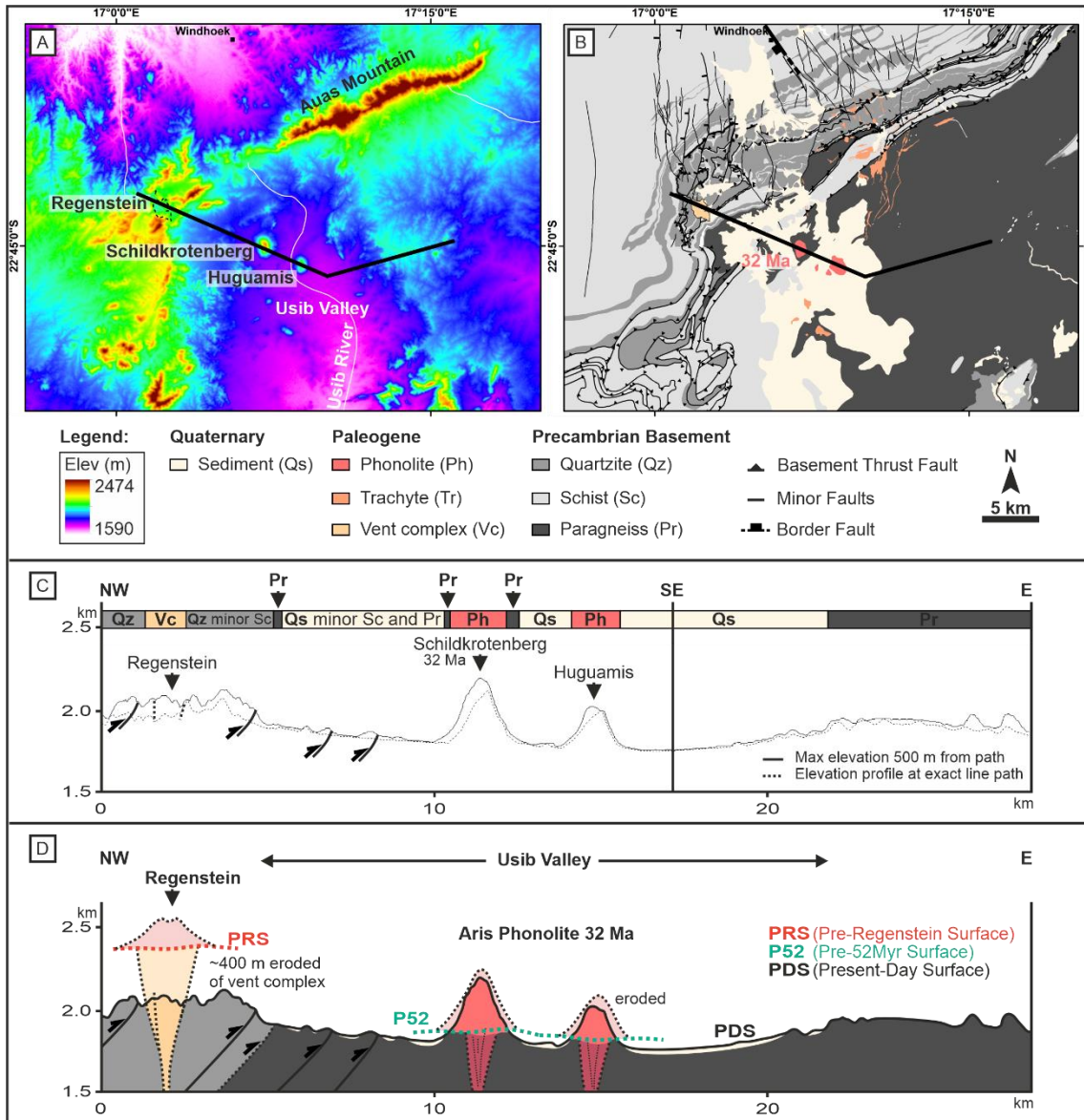
748

749 **Figure 5.** (A) SW-NE topographic profile of Windhoek and Swakop grabens showing the four  
 750 major bounding faults. Lithology distribution is added on top of the profile (lithology taken from  
 751 1:250,000 Namibia Geological Map sheets 2116 and 2216). (B) A longitudinal river profile of  
 752 scarp drainage (ENE-SSW) depicts a stepped-down profile. See Fig.3A for location. (C) An  
 753 oblique aerial image shows a fault scarp morphology in the eastern margin of the Windhoek  
 754 Graben. See Fig.3A for location. (D) Orientation of minor faults in the southern Windhoek Graben  
 755 (measured from structural map presented by Hoffmann and Schreiber (2011)).



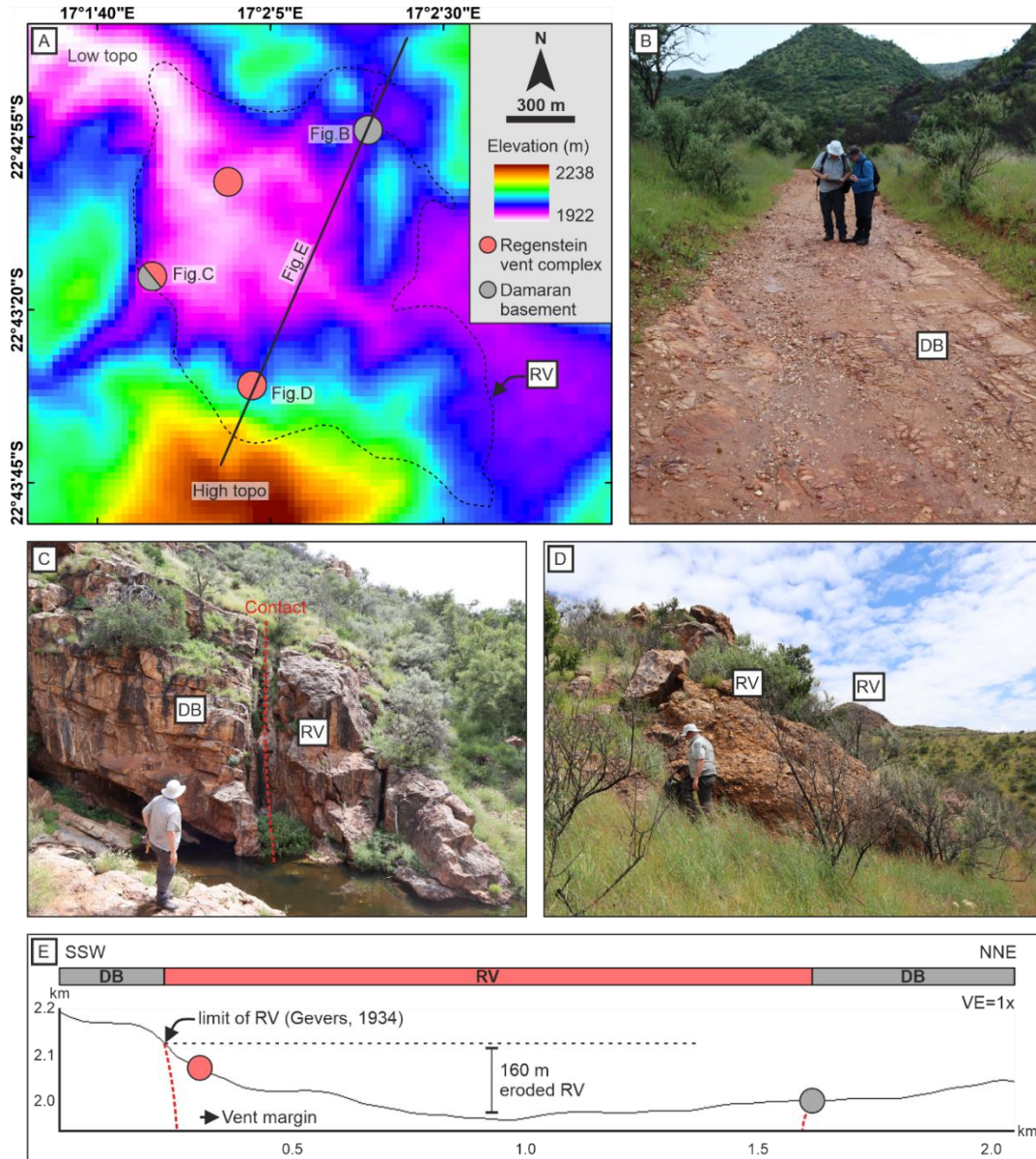
756

757 **Figure 6.** (A) Key faults (simplified from Fig. 3A) and igneous bodies (simplified from Gevers  
 758 (1932), Ferreira et al. (1979), and Marsh (2010)) are shown superimposed on the morphological  
 759 map. (B) Orientation of 162 dykes in southern Windhoek Graben (measured from maps of Miller  
 760 (2008), and the references therein). (C) Transverse and longitudinal topographic profiles of the  
 761 present-day valley of the Stalhart area.



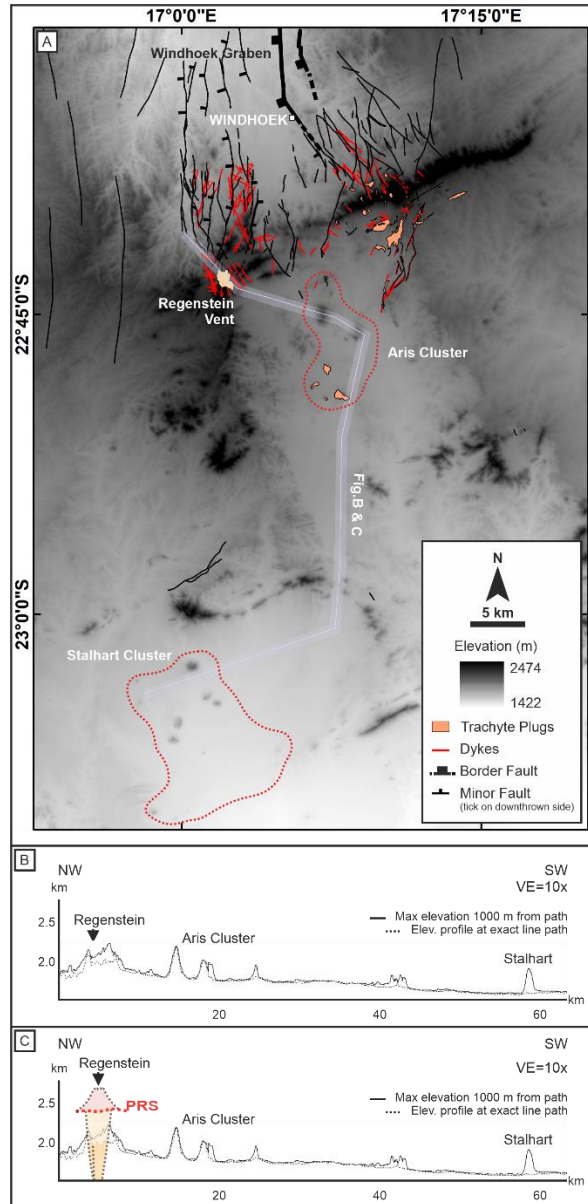
762

763 **Figure 7.** (A) Topographic map of vent complex (Regenstein) and Phonolites (Schildkrotenberg  
 764 and Huguamis) in the southern end of the Windhoek Graben. See Fig.6A for location. (B)  
 765 1:250,000 geological map of the area (sheet 2216, Geological Survey of Namibia). Dips direction  
 766 of the minor faults in southern Windhoek is adapted from Miller et al. (2018) (C) Uninterpreted  
 767 NW-E topographic profile of the vent complex and phonolites. The lateral geological distribution  
 768 of the 1:250,000 geological map is plotted on top of the profile. (D) Interpreted NW-E topographic  
 769 profile.



770

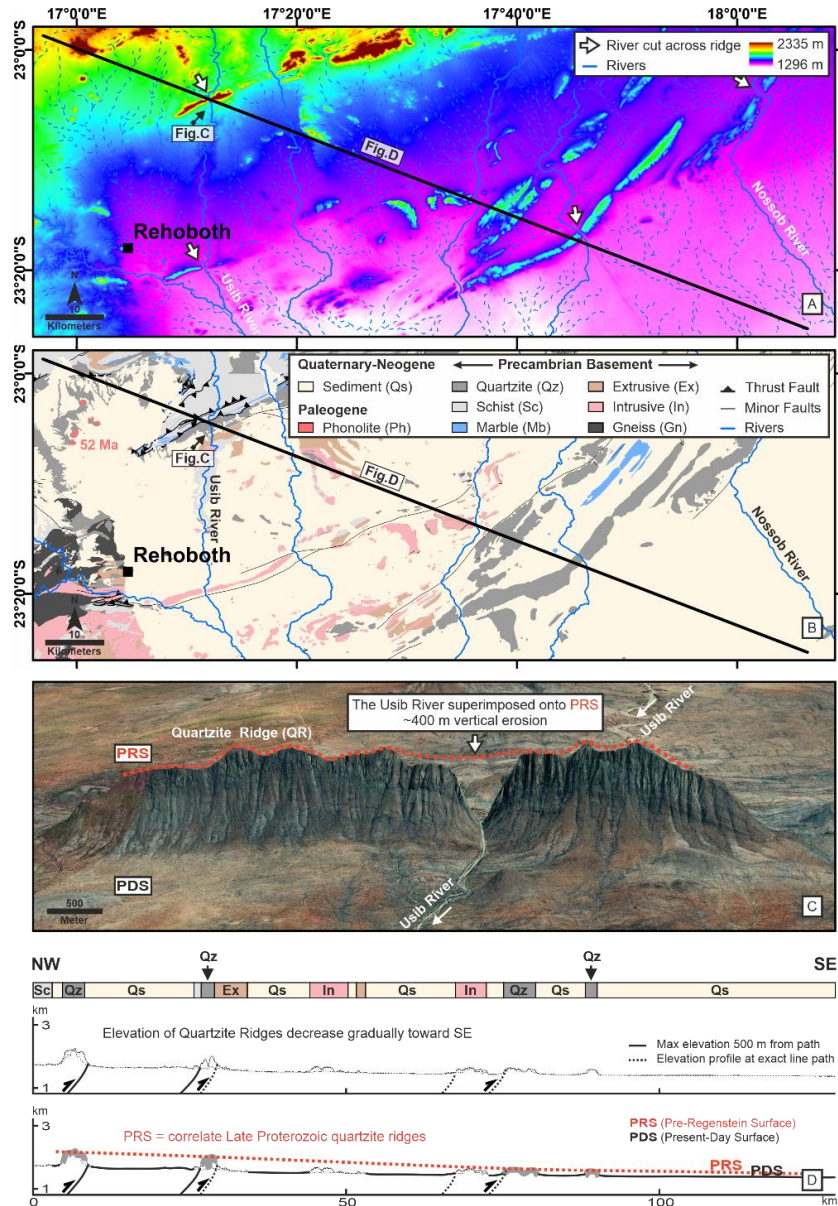
771 **Figure 8.** (A) Topographic map of the Regenstein vent complex (RV) with locations of field  
 772 photographs (B-D). (B) Field photograph taken just outside the main vent contact at the NW  
 773 margin of the Regenstein vent complex where weathered Damaran basement (DB) outcrops along  
 774 stream courses. (C) Field photograph showing a vertical contact between Damaran Basement and  
 775 Regenstein vent complex at the western margin of the vent. (D) Field photograph showing outcrop  
 776 of vent complex found at 2060 m in the southern area. (E) NNW-SSE topographic profile shows  
 777 ~160 m eroded of the Regenstein vent complex at the present-day surface.



778

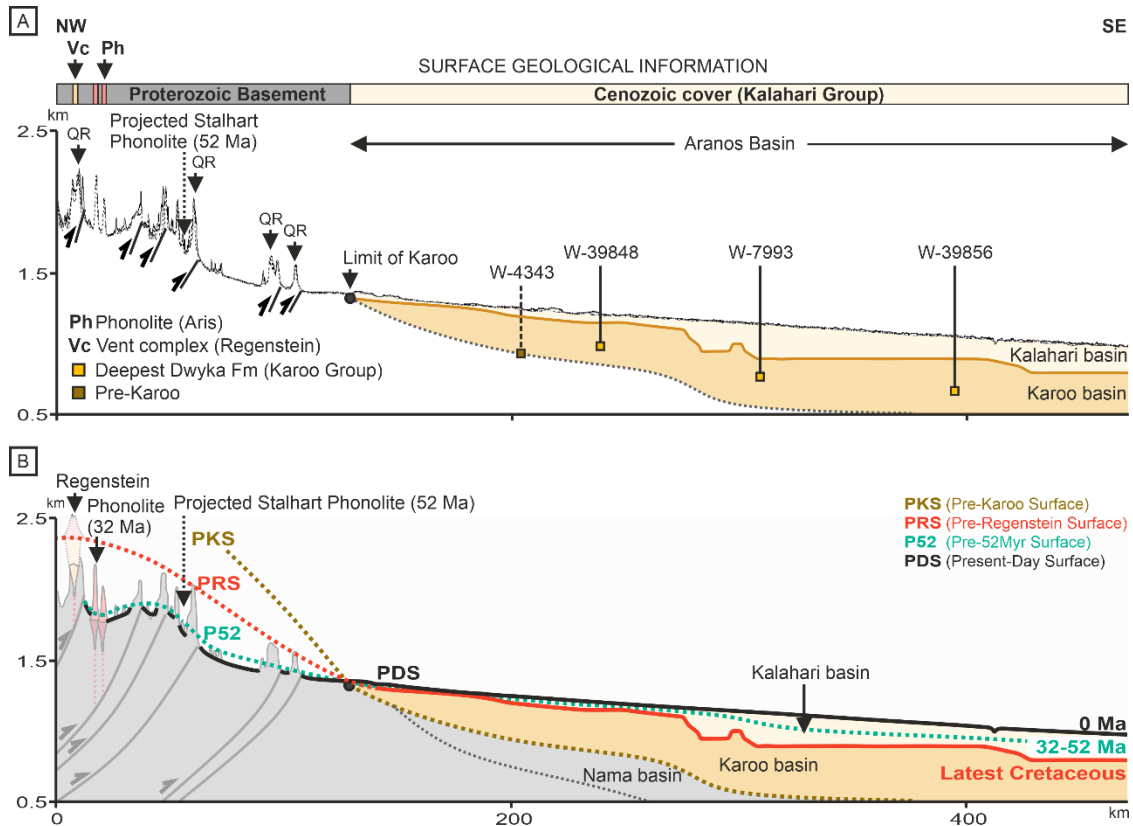
779 **Figure 9.** (A) Topographic map overlain by the southern faults of the Windhoek Graben (compiled  
 780 from Miller and Schalk (1980) and Hoffmann and Schreiber (2011)), dykes, trachytes, and  
 781 phonolites (compiled from Miller (2008) and the references therein), and Regensteen vent complex  
 782 (digitized from Hoffmann and Schreiber (2011)). Dip direction of the minor faults in southern  
 783 Windhoek is adapted from Miller et al. (2018) (B) Uninterpreted topographic profile from  
 784 Regensteen vent complex, Aris cluster, to Stalhart cluster. (C) Interpreted topographic profile of  
 785 (B). PRS: Pre-Regenstein Surface. See (A) for location.





786

787 **Figure 10.** (A) Topographic map of Rehoboth area showing rivers that cut across WSW ridges  
 788 (white arrows). See Fig.6A for location. (B) 1:250,000 geological map of the Rehoboth area  
 789 (Sheet: 2316, Geological Survey of Namibia). Note: Stalhart phonolites are located in the NW  
 790 area. Age is taken from Marsh et al. (2018). (C) Oblique satellite image showing the Usib River  
 791 cutting across the WSW quartzite ridge. See panel B for location. (D) Upper: uninterpreted NW-  
 792 SE topographic profile shows decreasing elevation of quartzite ridges towards the SE. Lower:  
 793 interpreted section of the PRS.



794

795 **Figure 11.** (A) Uninterpreted NW-SE topographic profile from the southernmost Windhoek  
 796 Graben (Regenstein area) to the Aranos Basin. See Fig.2A for location. Surface geological  
 797 information is added on top of the profile (Adapted from Miller and Schalk (1980) and Hoffmann  
 798 and Schreiber (2011)). The bases of Kalahari and Karoo basins are drawn based on borehole  
 799 information in the Aranos Basin presented by Miller (2008). (B) The interpreted section shows the  
 800 relationship between key surfaces in the highlands and the Aranos Basin.

801

802 **REFERENCE CITED**

803 Aizawa, M., Bluck, B., Cartwright, J., Milner, S., Swart, R., and Ward, J., 2000, Constraints on  
 804 the geomorphological evolution of Namibia from the offshore stratigraphic record.  
 805 Communications of the Geological Survey of Namibia, v. 12, p. 337-346.  
 806 Al-Hajri, Y., White, N., and Fishwick, S., 2009, Scales of transient convective support beneath  
 807 Africa. *Geology*, v. 37, no. 10, p. 883-886. <https://doi.org/10.1130/G25703A.1>  
 808 Baby, G., Guillocheau, F., Braun, J., Robin, C., and Dall'Asta, M., 2020, Solid sedimentation rates  
 809 history of the Southern African continental margins: Implications for the uplift history of

- 810 the South African Plateau. *Terra Nova*, v. 32, no. 1, p. 53-65.  
 811 <https://doi.org/10.1111/ter.12435>
- 812 Barnes, S.-J., and Sawyer, E. W., 1980, An alternative model for the Damara mobile belt: ocean  
 813 crust subduction and continental convergence. *Precambrian Research*, v. 13, no. 4, p. 297-  
 814 336. [https://doi.org/10.1016/0301-9268\(80\)90048-0](https://doi.org/10.1016/0301-9268(80)90048-0)
- 815 Bluck, B., Ward, J., Cartwright, J., and Swart, R., 2007, The Orange River, southern Africa: an  
 816 extreme example of a wave-dominated sediment dispersal system in the South Atlantic  
 817 Ocean. *Journal of the Geological Society*, v. 164, no. 2, p. 341-351.  
 818 <https://doi.org/10.1144/0016-76492005-189>
- 819 Burger, A. J., and Walraven, T., 1976, Summary of the age determinations carried out during the  
 820 period April 1975 to March 1976. *Annals of the Geological Survey of South Africa*, v. 11,  
 821 p. 323-329.
- 822 Burke, K., 1996, The African Plate. *South African Journal of Geology*, v. 99, no. 4, p. 341-409.  
 823 <https://hdl.handle.net/10520/EJC-942801f20>
- 824 Burke, K., and Gunnell, Y., 2008, The African erosion surface: a continental-scale synthesis of  
 825 geomorphology, tectonics, and environmental change over the past 180 million years.  
 826 *Geological Society of America*, v. 201, p. 66.
- 827 Clemson, J., Cartwright, J., and Booth, J., 1997, Structural segmentation and the influence of  
 828 basement structure on the Namibian passive margin. *Journal of the Geological Society*, v.  
 829 154, no. 3, p. 477-482. <https://doi.org/10.1144/gsjgs.154.3.0477>
- 830 Daly, M., Green, P., Watts, A., Davies, O., Chibesakunda, F., and Walker, R., 2020, Tectonics and  
 831 landscape of the Central African Plateau and their implications for a propagating  
 832 Southwestern Rift in Africa. *Geochemistry, Geophysics, Geosystems*, v. 21, no. 6, p.  
 833 e2019GC008746. <https://doi.org/10.1029/2019GC008746>
- 834 de Kock, G. S., 1992, Forearc basin evolution in the Pan-African Damara Belt, central Namibia:  
 835 the Hureb formation of the Khomas zone. *Precambrian Research*, v. 57, no. 3-4, p. 169-  
 836 194. [https://doi.org/10.1016/0301-9268\(92\)90001-5](https://doi.org/10.1016/0301-9268(92)90001-5)
- 837 De Kock, W., 1934, The geology of the western Rehoboth. *South West Africa Department of*  
 838 *Mines Memoir*, v. 1, p. 147.
- 839 De Wit, M., 2007, The Kalahari Epeirogeny and climate change: differentiating cause and effect  
 840 from core to space. *South African Journal of Geology*, v. 110, no. 2-3, p. 367-392.  
 841 <https://doi.org/10.2113/gssajg.110.2-3.367>
- 842 Downing, K. N., and Coward, M., 1981, The Okahandja Lineament and its significance for  
 843 Damaran tectonics in Namibia. *Geologische Rundschau*, v. 70, no. 3, p. 972-1000.
- 844 Ferreira, C., Jacob, R., and Marsh, J., 1979, Base-metal mineralization in alkaline pyroclastics-the  
 845 Regenstein vent, South West Africa. *South African Journal of Geology*, v. 82, no. 2, p.  
 846 243-249.
- 847 Gallagher, K., and Brown, R., 1999, The Mesozoic denudation history of the Atlantic margins of  
 848 southern Africa and southeast Brazil and the relationship to offshore sedimentation.  
 849 *Geological Society, London, Special Publications*, v. 153, no. 1, p. 41-53.  
 850 <https://doi.org/10.1098/rsta.1999.0354>
- 851 Gawthorpe, R., and Leeder, M., 2000, Tectono-sedimentary evolution of active extensional basins.  
 852 *Basin Research*, v. 12, no. 3-4, p. 195-218. <https://doi.org/10.1111/j.1365-2117.2000.00121.x>
- 854 Gevers, T., 1932, The hot springs of Windhoek, SW Africa. *South African Journal of Geology*, v.  
 855 35, no. 01, p. 1-28.

- 856 -, 1934, Alkali-rocks in the Auas Mountains, south of Windhoek, SWA. Transactions of the  
857 Geological Society of South Africa, v. 36, p. 77-88.
- 858 -, 1942, The Morphology of the Windhoek District, South West Africa. South African  
859 Geographical Journal, v. 24, no. 1, p. 45-64.
- 860 Gladchenko, T., Hinz, K., Eldholm, O., Meyer, H., Neben, S., and Skogseid, J., 1997, South  
861 Atlantic volcanic margins. Journal of the Geological Society, v. 154, no. 3, p. 465-470.  
862 <https://doi.org/10.1144/gsjgs.154.3.0465>
- 863 Goldsworthy, M., and Jackson, J., 2000, Active normal fault evolution in Greece revealed by  
864 geomorphology and drainage patterns. Journal of the Geological Society, v. 157, no. 5, p.  
865 967-981. <https://doi.org/10.1144/jgs.157.5.967>
- 866 Gray, D. R., Foster, D., Meert, J., Goscombe, B., Armstrong, R., Trouw, R., and Passchier, C.,  
867 2008, A Damara orogen perspective on the assembly of southwestern Gondwana.  
868 Geological Society, London, Special Publications, v. 294, no. 1: West Gondwana: Pre-  
869 Cenozoic Correlations Across the South Atlantic Region, p. 257-278.  
870 <https://doi.org/10.1144/SP294.14>
- 871 Guj, P., 1967, Structural geology of the Auas Mountains, Windhoek District, South West Africa.  
872 Annals of the Geological Survey of South Africa, Pretoria, v. 6, p. 55-66.
- 873 Haddon, I., and McCarthy, T., 2005, The Mesozoic–Cenozoic interior sag basins of Central Africa:  
874 the late-cretaceous–Cenozoic Kalahari and Okavango basins. Journal of African Earth  
875 Sciences, v. 43, no. 1-3, p. 316-333. <https://doi.org/10.1016/j.jafrearsci.2005.07.008>
- 876 Hartmann, K., 1994, Tectonic and structural aspects at the Otjihase Mine, Matchless belt, Namibia  
877 [M.Sc.: Rhodes University, 101 p.
- 878 Hodge, M., Biggs, J., Fagereng, Å., Mdala, H., Wedmore, L., and Williams, J., 2020, Evidence  
879 from high-resolution topography for multiple earthquakes on high slip-to-length fault  
880 scarps: The Bilila-Mtakataka Fault, Malawi. Tectonics, v. 39, no. 2, p. e2019TC005933.  
881 <https://doi.org/10.1029/2019TC005933>
- 882 Hoffmann, K., and Schreiber, U., 1998, Geological Map 2216 - Windhoek. Provisional Open File  
883 geol. map 1:250 000 series. Geological Survey of Namibia.
- 884 Hoffmann, K. H., 1983, Lithostratigraphy and facies of the Swakop Group of the southern Damara  
885 Belt, SWA/Namibia. In: Miller, R.M. (ed) Evolution of the Damara Orogen of South West  
886 Africa/Namibia. Geological Society of South Africa Special Publication, v. 11, p. 43-63.
- 887 Hoffmann, K. H., and Schreiber, U. M., 2011, Geological map 2217CA - Windhoek 1:50.000.  
888 Geological Survey of Namibia.
- 889 Jacob, R. J., 2005, The erosional and Cainozoic depositional history of the Lower Orange River,  
890 southwestern Africa. Doctoral dissertation, University of Glasgow.
- 891 Kasch, K., 1986, Tectonic subdivision, lithostratigraphy and structural geology of the Upper Black  
892 Nossob River area. Communications of the Geological Survey of South West  
893 Africa/Namibia, v. 2, p. 117-129.
- 894 Kinabo, B. D., Atekwana, E. A., Hogan, J. P., Modisi, M. P., Wheaton, D. D., and Kampunzu, A.,  
895 2007, Early structural development of the Okavango rift zone, NW Botswana. Journal of  
896 African Earth Sciences, v. 48, no. 2-3, p. 125-136.  
897 <https://doi.org/10.1016/j.jafrearsci.2007.02.005>
- 898 Kukla, P. A., 1992, Tectonics and sedimentation of late Proterozoic Damaran convergent  
899 continental margin, Khomas Hochland, central Namibia. Geological Survey of Namibia  
900 Memoir v. 12, p. 95 pp.

- 901 Leeder, M., and Jackson, J., 1993, The interaction between normal faulting and drainage in active  
902 extensional basins, with examples from the western United States and central Greece.  
903 Basin Research, v. 5, no. 2, p. 79-102. <https://doi.org/10.1111/j.1365-2117.1993.tb00059.x>
- 904 Mabbutt, J., 1951, The evolution of the middle Ugab valley, Damaraland, south west Africa.  
905 Transactions of the Royal Society of South Africa, v. 33, no. 3, p. 333-363.  
906 <https://doi.org/10.1080/00359195109519890>
- 907 Marsh, J., 2010, The geochemistry and evolution of Palaeogene phonolites, central Namibia.  
908 Lithos, v. 117, no. 1-4, p. 149-160. <https://doi.org/10.1016/j.lithos.2010.02.012>
- 909 Marsh, J., Phillips, D., and Lock, B., 2018, 40Ar/39Ar dating of the Klinghardt and Stalhart  
910 Phonolites, Namibia, and Comments on the Evolution of the Klinghardt Volcanic Field.  
911 Communications of the Geological Survey of Namibia, v. 20, p. 1-8.
- 912 Martin, H., 1973, The Atlantic margin of southern Africa between latitude 17 south and The Cape  
913 of Good Hope. In: Nairn, A.E.M., Stehli, F.G. (ed) The South Atlantic. Springer, p. 277-  
914 300. [https://doi.org/10.1007/978-1-4684-3030-1\\_7](https://doi.org/10.1007/978-1-4684-3030-1_7)
- 915 Martin, H., and Porada, H., 1977, The intracratonic branch of the Damara orogen in South West  
916 Africa I. Discussion of geodynamic models. Precambrian Research, v. 5, no. 4, p. 311-338.  
917 [https://doi.org/10.1016/0301-9268\(77\)90039-0](https://doi.org/10.1016/0301-9268(77)90039-0)
- 918 Matmon, A., Enzel, Y., Vainer, S., Grodek, T., Mushkin, A., and Team, A., 2018, The near steady  
919 state landscape of western Namibia. Geomorphology, v. 313, p. 72-87.  
920 <https://doi.org/10.1016/j.geomorph.2018.04.008>
- 921 Miller, R. M., 1983, The Pan-African Damara Orogen of South West Africa/Namibia. In: Miller,  
922 R.M., (ed) Evolution of the Damara orogen of South West Africa/Namibia. Geological  
923 Society of South Africa Special Publication, v. 11, p. 431-515.
- 924 Miller, R. M., 2008, The geology of Namibia. Ministry of Mines and Energy, Windhoek. v. 3, pp  
925 1566.
- 926 Miller, R. M., Carr, R., Van Der Merwe, B., Symons, G., Murray, R., and Amputu, M., 2018,  
927 Some Geological and Geophysical Aspects of the 2016/2017 Drilling Campaign in the  
928 Windhoek Aquifer. Communications of the Geological Survey of Namibia, v. 19, p. 8-19.
- 929 Miller, R. M., and Schalk, K. E. L., 1980, Geological map of Namibia 1:1.000.000. Geological  
930 Survey of Namibia.
- 931 Moore, A., 1999, A reappraisal of epeirogenic flexure axes in southern Africa. South African  
932 Journal of Geology, v. 102, no. 4, p. 363-376.
- 933 Moore, A., Blenkinsop, T., and Cotterrill, F., 2008, Controls on post-Gondwana alkaline  
934 volcanism in Southern Africa. Earth Planetary Science Letters, v. 268, no. 1-2, p. 151-164.  
935 <https://doi.org/10.1016/j.epsl.2008.01.007>
- 936 Morley, C., 1988, Variable extension in lake Tanganyika. Tectonics, v. 7, no. 4, p. 785-801.  
937 <https://doi.org/10.1029/TC007i004p00785>
- 938 Morley, C., Nelson, R., Patton, T., and Munn, S., 1990, Transfer zones in the East African rift  
939 system and their relevance to hydrocarbon exploration in rifts. AAPG Bulletin, v. 74, no.  
940 8, p. 1234-1253. <https://doi.org/10.1306/OC9B2475-1710-11D7-8645000102C1865D>
- 941 Mvondo, F., Dauteuil, O., and Guillocheau, F., 2011, The Fish River canyon (Southern Namibia):  
942 a record of Cenozoic mantle dynamics? Comptes Rendus Geoscience, v. 343, no. 7, p. 478-  
943 485. <https://doi.org/10.1016/j.crte.2011.07.003>
- 944 Niku Paavola, V., 1997, Alkaline rocks of the Aris area, central Namibia. Unpublished MSc thesis,  
945 University of Helsinki, 71pp.

- 946 Nyblade, A. A., and Sleep, N. H., 2003, Long lasting epeirogenic uplift from mantle plumes and  
 947 the origin of the Southern African Plateau. *Geochemistry, Geophysics, Geosystems*, v. 4,  
 948 no. 12. <https://doi.org/10.1029/2003GC000573>
- 949 Partridge, T., and Maud, R., 1987, Geomorphic evolution of southern Africa since the Mesozoic.  
 950 *South African Journal of Geology*, v. 90, no. 2, p. 179-208.
- 951 Partridge, T. C., 1998, Of diamonds, dinosaurs and diastrophism: 150 million years of landscape  
 952 evolution in southern Africa. *South African Journal of Geology*, v. 101, no. 3, p. 167-184.
- 953 Picart, C., Dauteuil, O., Pickford, M., and Owono, F. M., 2020, Cenozoic deformation of the South  
 954 African plateau, Namibia: Insights from planation surfaces. *Geomorphology*, v. 350, p.  
 955 106922. <https://doi.org/10.1016/j.geomorph.2019.106922>
- 956 Ponte, J.-P., Robin, C., Guillocheau, F., Popescu, S., Suc, J.-P., Dall'Asta, M., Melinte-  
 957 Dobrinescu, M. C., Bubik, M., Dupont, G., and Gaillot, J., 2019, The Zambezi delta  
 958 (Mozambique channel, East Africa): High resolution dating combining bio-orbital and  
 959 seismic stratigraphies to determine climate (palaeoprecipitation) and tectonic controls on a  
 960 passive margin. *Marine and Petroleum Geology*, v. 105, p. 293-312.  
 961 <https://doi.org/10.1016/j.marpetgeo.2018.07.017>
- 962 Porada, H., 1989, Pan-African rifting and orogenesis in southern to equatorial Africa and eastern  
 963 Brazil. *Precambrian Research*, v. 44, no. 2, p. 103-136. [https://doi.org/10.1016/0301-](https://doi.org/10.1016/0301-9268(89)90078-8)  
 964 [9268\(89\)90078-8](https://doi.org/10.1016/0301-9268(89)90078-8)
- 965 Raab, M. J., Brown, R. W., Gallagher, K., Carter, A., and Weber, K., 2002, Late Cretaceous  
 966 reactivation of major crustal shear zones in northern Namibia: constraints from apatite  
 967 fission track analysis. *Tectonophysics*, v. 349, no. 1-4, p. 75-92.  
 968 [https://doi.org/10.1016/S0040-1951\(02\)00047-1](https://doi.org/10.1016/S0040-1951(02)00047-1)
- 969 Rosendahl, B., Reynolds, D., Lorber, P., Burgess, C., McGill, J., Scott, D., Lambiase, J., and  
 970 Derksen, S., 1986, Structural expressions of rifting: lessons from Lake Tanganyika, Africa.  
 971 *Geological Society, London, Special Publications*, v. 25, no. 1: Sedimentation in the  
 972 African Rifts, p. 29-43. <https://doi.org/10.1144/GSL.SP.1986.025.01.04>
- 973 Trudgill, B., and Cartwright, J., 1994, Relay-ramp forms and normal-fault linkages, Canyonlands  
 974 National Park, Utah. *Geological Society of America Bulletin*, v. 106, no. 9, p. 1143-1157.  
 975 [https://doi.org/10.1130/0016-7606\(1994\)106%3C1143:RRFANF%3E2.3.CO;2](https://doi.org/10.1130/0016-7606(1994)106%3C1143:RRFANF%3E2.3.CO;2)
- 976 Wallace, R. E., 1977, Profiles and ages of young fault scarps, north-central Nevada. *Geological*  
 977 *Society of America Bulletin*, v. 88, no. 9, p. 1267-1281. [https://doi.org/10.1130/0016-](https://doi.org/10.1130/0016-7606(1977)88%3C1267:PAAOYF%3E2.0.CO;2)  
 978 [7606\(1977\)88%3C1267:PAAOYF%3E2.0.CO;2](https://doi.org/10.1130/0016-7606(1977)88%3C1267:PAAOYF%3E2.0.CO;2)
- 979 Ward, J., 1988, Eolian, fluvial and pan (playa) facies of the Tertiary Tsondab Sandstone Formation  
 980 in the central Namib Desert, Namibia. *Sedimentary Geology*, v. 55, no. 1-2, p. 143-162.  
 981 [https://doi.org/10.1016/0037-0738\(88\)90094-2](https://doi.org/10.1016/0037-0738(88)90094-2)
- 982 Wildman, M., Gallagher, K., Chew, D., and Carter, A., 2021, From sink to source: Using offshore  
 983 thermochronometric data to extract onshore erosion signals in Namibia. *Basin Research*,  
 984 v. 33, no. 2, p. 1580-1602. <https://doi.org/10.1111/bre.12527>
- 985